การเตรียมตัวเร่งปฏิกิริยานิกเกิลบนเส้นใยซิลิกาสำหรับการรีฟอร์มกลีเซอรอลด้วยไอน้ำ

นางสาวณัฐธิดา ตั้งคณาพร

วิทยานิพนธ์นี้เป็นส่วนหนึ่งของการศึกษาตามหลักสูตรปริญญาวิทยาศาสตรมหาบัณฑิต
สาขาวิชาปิโตรเคมีและวิทยาศาสตร์พอลิเมอร์
คณะวิทยาศาสตร์ จุฬาลงกรณ์มหาวิทยาลัย
ปีการศึกษา 2552

PREPARATION OF Ni/SiO₂ FIBER CATALYSTS FOR STEAM REFORMING OF GLYCEROL

Miss Nattida Tangkanaporn

ศูนย์วิทยทรัพยากร

จุฬาลงกรณ์มหาวิทยาลัย

A Thesis Submitted in Partial Fulfillment of the Requirements
for the Degree of Master of Science in Petrochemistry and Polymer Science
Faculty of Science
Chulalongkorn University
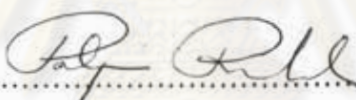Academic Year 2009
Copyright of Chulalongkorn University

520194

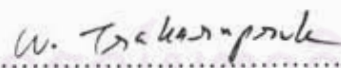|	
Thesis Title	PREPARATION OF Ni/SiO$_2$ FIBER CATALYSTS FOR STEAM REFORMING OF GLYCEROL
By	Miss Nattida Tangkanaporn
Field of Study	Petrochemistry and Polymer Science
Thesis Advisor	Assistant Professor Prasert Reubroychareon

Accepted by the Faculty of Science, Chulalongkorn University in Partial Fulfillment of the Requirements for the Master's Degree

.....................................Dean of the Faculty of Science

(Professor Supot Hannongbua, Dr.rer.nat.)

THESIS COMMITTEE

.....................................Chairman

(Professor Pattarapan Prasassarakich, Ph.D.)

.....................................Thesis Advisor

(Assistant Professor Prasert Reubroychareon, D.Eng.)

.....................................Examiner

(Associate Professor Wimonrat Trakarnpruk, Ph.D.)

.....................................External Examiner

(Chanathip Samart, D.Eng.)

ณัฐธิดา ตังคณาพร : การเตรียมตัวเร่งปฏิกิริยานิกเกิลบนเส้นใยซิลิกาสำหรับการรีฟอร์ม
กลีเซอรอลด้วยไอน้ำ. (PREPARATION OF Ni/SiO$_2$ FIBER CATALYSTS FOR STEAM
REFORMING OF GLYCEROL) อ. ที่ปรึกษาวิทยานิพนธ์หลัก : ผศ.คร. ประเสริฐ เรียบร้อย
เจริญ, 89 หน้า.

จุดประสงค์หลักของงานวิจัยนี้คือ การเตรียมตัวเร่งปฏิกิริยานิกเกิลบนเส้นใยซิลิกาสำหรับการ
รีฟอร์มกลีเซอรอลด้วยไอน้ำ ตัวเร่งปฏิกิริยานิกเกิลบนตัวรองรับเส้นใยซิลิกาสามารถเตรียมได้ด้วยวิธี
โซลเจล ร่วมกับเทคนิคอิเล็กโทรสปินนิง จากนั้นเส้นใยซิลิกาจะถูกเอิบชุ่มด้วยสารละลายนิกเกิล ซึ่งใน
งานวิจัยนี้สนใจศึกษาตัวแปร คือ ค่าความต่างศักย์ และระยะห่างระหว่างปลายเข็มถึงฉากที่มีต่อสัณฐาน
วิทขาของเส้นใย โดยพิสูจน์เอกลักษณ์ของตัวเร่งปฏิกิริยาด้วยเทคนิค SEM EDS TEM XRD และ TPR
ผลการวิเคราะห์ SEM แสดงให้เห็นว่า ภาวะการเตรียมเส้นใยซิลิกาที่ค่าความต่างศักย์ 25 กิโลโวลต์และ
ระยะห่างระหว่างปลายเข็มถึงฉาก 15 เซนติเมตร จะให้เส้นใยที่มีค่าเส้นผ่านศูนย์กลางเล็กที่สุด เท่ากับ
0.93 ไมโครเมตร จากการตรวจสอบปริมาณนิกเกิลด้วยเทคนิค EDS พบว่า ร้อยละนิกเกิลบนตัวรองรับซิ
ลิกามีค่าใกล้เคียงกับที่ต้องการเตรียม ผลการวิเคราะห์ XRD ของตัวเร่งปฏิกิริยาแสดงให้เห็นว่า ตัวเร่ง
ปฏิกิริยามีโครงสร้างอสัณฐานของเส้นใยซิลิกาและโครงสร้างผลึกของนิกเกิล จากการนำตัวเร่งปฏิกิริยา
ไปทดสอบการเร่งปฏิกิริยาการรีฟอร์มกลีเซอรอลด้วยไอน้ำ โดยศึกษาปัจจัยที่มีผลต่อปฏิกิริยา เช่น
อุณหภูมิ อัตราสารป้อนเข้า อัตราส่วนน้ำต่อกลีเซอรอล ปริมาณโลหะนิกเกิลและการเติมโลหะซีเรียม
เป็นต้น ผลการทดสอบพบว่า ตัวเร่งปฏิกิริยาชนิดเส้นใยจะให้ค่าการเปลี่ยนกลีเซอรอลสูงกว่าตัวเร่ง
ปฏิกิริยาชนิดรูพรุน โดยเลือกเกิดก๊าซผลิตภัณฑ์หลัก คือก๊าซไฮโดรเจนและก๊าซคาร์บอนมอนอกไซค์
สำหรับตัวเร่งปฏิกิริยาชนิดรูพรุน จะเลือกเกิดก๊าซไฮโดรเจนและก๊าซคาร์บอนไดออกไซด์เป็นผลิตภัณฑ์
หลัก เนื่องมาจากตัวรองรับซิลิกาต่างชนิดกัน จะมีคุณสมบัติการดูดซับน้ำที่แตกต่างกัน ซึ่งตัวรองรับชนิด
ซิลิกาเส้นใยที่จะสามารถดูดซับน้ำได้น้อยกว่าตัวรองรับซิลิกาชนิดรูพรุน จึงส่งผลให้ตัวเร่งปฏิกิริยาชนิด
เส้นใยดูดซับโมเลกุลน้ำไม่เพียงพอต่อการทำปฏิกิริยากับก๊าซคาร์บอนมอนอกไซค์ด้วยปฏิกิริยาวอร์เตอร์
ก๊าซชิฟ ที่ซึ่งเป็นปฏิกิริยาการเปลี่ยนก๊าซคาร์บอนมอนอกไซค์กับน้ำไปอยู่ในรูปของก๊าซ
คาร์บอนไดออกไซด์ กับก๊าซไฮโดรเจน ดังนั้นตัวเร่งปฏิกิริยาชนิดเส้นใย จึงผลิตก๊าซไฮโดรเจนและก๊าซ
คาร์บอนมอนอกไซด์ เป็นผลิตภัณฑ์หลัก

ภาควิชา ปิโตรเคมีและวิทยาศาสตร์พอลิเมอร์   ลายมือชื่อนิสิต

สาขาวิชา ปิโตรเคมีและวิทยาศาสตร์พอลิเมอร์   ลายมือชื่ออ.ที่ปรึกษาวิทยานิพนธ์หลัก

ปีการศึกษา 2552

5072268123   : MAJOR PETROCHEMISTRY AND POLYMER SCIENCE

KEYWORDS : ELECTROSPINNING / FIBER CATALYSTS / GLYCEROL STEAM REFORMING

NATTIDA TANGKANAPORN : PREPARATION OF Ni/SiO$_2$ FIBER CATALYSTS FOR STEAM REFORMING OF GLYCEROL. THESIS ADVISOR : ASSIST. PROF. PRASERT REUBROYCHAREON, Ph.D., 89 pp.

This work is aimed to prepare nickel/silica fiber catalyst for steam reforming reaction of glycerol. The nickel/silica fiber catalyst was prepared by a sol-gel and electrospinning technique and then the silica fiber was impregnated by nickel solution. The effects of processing parameters on the morphology of silica fibers such as spinning voltage and the tip to collector distance were studied. The catalysts were characterized by SEM, EDS, TEM, XRD, and TPR. SEM results showed that the average diameter of silica fiber prepared by the applied voltage 15 kV and tip to collector distance 25 cm was the smallest of 0.93 μm. The amount of Ni measured by EDS technique was close to that of Ni loaded by impregnation. The XRD pattern of nickel/silica fiber catalyst showed the amorphous structure of pure silica fibers and the crystalline structure for nickel. The catalyst activity tests on glycerol steam reforming reaction were studied. The reaction parameters such as temperature, feed flow rate, water/glycerol mole ratio, the nickel content, and the additional cerium were investigated. The fiber catalyst showed the higher glycerol conversion compared with the porous catalyst at the same reaction condition and produced H$_2$ and CO as main products whereas the porous catalyst produced H$_2$ and CO$_2$ as main products. This can be attributed to the different silica support adsorbing water differently. The silica fiber support adsorbed water lower than the porous support thus the fiber catalyst may not have the water molecules enough to react with CO by water gas shift which converted CO and water into CO$_2$ and H$_2$. Therefore the fiber catalyst produced H$_2$ and CO as the main products.

Field of Study : Petrochemistry and Polymer Science   Student's Signature _Nattida Tangkanaporn_

Academic Year :   2009   Advisor's Signature _P.h_

ACKNOWLEDGEMENTS

CONTENTS

x

page

ศูนย์วิทยทรัพยากร
จุฬาลงกรณ์มหาวิทยาลัย

LIST OF TABLES

LIST OF FIGURES

ศูนย์วิทยทรัพยากร
จุฬาลงกรณ์มหาวิทยาลัย

ต้นฉบับไม่มีหน้านี้
NO THIS PAGE IN ORIGINAL

CHAPTER I

INTRODUCTION

1.1 Background

One of the major energy resources is fossil fuels. Since the worldwide energy need has increased exponentially, the reserves of fossil fuels decreased. This resource also has serious negative effects on environment because of gas pollution. Thus, considerable attention was focused on the development of alternative energy source. Various alternative fuels such as hydrogen, ethanol and biodiesel are being exploited currently to sustain the energy requirement.

Hydrogen (H_2) is forecast to become a major source of energy in the future. Molecular hydrogen is a clean burning fuel, considered as an alternative fuel which provides energy for fuel cell (FC) applications as in automotive applications or electricity production. Hydrogen is also an important material for chemical synthesis and refinery for clean fuel production [1].

Currently, steam reforming of natural gas is a largest and generally the most economical way to produce hydrogen [2]. However, the natural gas is a non-renewable source. Thus, the steam reforming of biomass represents an interested source being environmental and political concerns.

Glycerol is a waste by-product from transesterification process to produce biodiesel, one of the alternative fuels which less emitted carbon dioxide when compared to regular diesel fuel, about 10wt% of vegetable oils converted into glycerol. It may represent a potential feedstock for hydrogen production. Glycerol can be efficiently converted in hydrogen by means of its catalytic reaction with steam. Nickel based catalysts has attracted to be considerable attention owing to its good catalytic performance and low price [16]. The

kind of catalyst support is one of influent reaction factors. Generally, steam reforming reaction occurs at surface of the porous catalyst where the reaction rate may be affected by glycerol transfer into pore. Moreover, formation of carbon will cause loss of effective surface area, lower heat transfer from catalyst to gas, and plug of the void space. Therefore, to keep off these effects we expect to find new kind of support as fiber which has no pore and high surface area per volume that becomes to be support for catalyst without the diffusion and pore blockage problems.

Nowadays, fiber can be produced by electrospinning technique, is commonly used for producing metal oxide and/or nonwoven polymer fiber. Since electrospun fiber normally have diameters ranged from sub-micrometers down to nanometers, their surface area per volume ratios are very large. These organic or inorganic fiber are interesting for a variety of applications including semi-permeable membrane, fiber, composite reinforcement, optical and electronic devices.

This work can be divided into two main experimental parts. The first is the electrospinning of silica fiber as support for the catalyst. In this part, the effect of applied voltage and tip to collector distance (TCD) on morphological appearance of silica fibers was thoroughly investigated, using scanning electron microscopy. The second is to study the catalytic performance of the obtained fibers which impregnated with nickel acetate for steam reforming of glycerol.

1.2 Objective

The objective of this research is to develop the fiber catalysts which are suitable for steam reforming process from glycerol. In this investigation, process conditions will be optimized by studying the effect of temperature, water glycerol mole ratio, feed flow rate, the nickel loading and the additional cerium loading.

1.3 Scope of the research

This research was to study the preparation of silica fiber by electrospinning technique that showed high surface area per volume ratio. The fiber support was impregnated with nickel acetate solution. The influence of this catalyst and the operating parameters, i.e. temperature, water glycerol mole ratio and feed flow rate on the performance in the steam reforming of glycerol were carried out. The research procedures were carried out as follows;

1. Literature review of this research work
2. Design and installation of steam reforming apparatus in laboratory scale and also preparation of the chemicals and raw materials for the experiment.
3. Study of the preparation conditions of silica fiber by electrospinning technique and characterization
   a. Applied voltage (15 20 and 25 kV)
   b. Tip to collector distance (10 15 and 20 cm)
4. Study of influence of nickel/silica fiber catalyst and operating parameters on the performance in the steam reforming of glycerol at atmospheric pressure:
   a. Temperature (550 650 and 750°C)
   b. Water glycerol mole ratio (3:1 6:1 and 9:1)
   c. Feed flow rate (0.01 0.03 and 0.05 mL/min)
   d. Weight percentage of nickel (5 10 and 20)
   e. Weight percentage of added cerium (1 and 2)

1.4 Expected results

The new kind of nickel/silica fiber catalyst with small size in diameter would be developed by sol-gel and electrospinning techniques and can be used as the good catalyst for steam reforming of glycerol which the diffusion and pore blockage problems might not be occurred.

CHAPTER II

THEORY AND LITERATURE REVIEWS

2.1 Electrospinning

The electrostatic spinning or 'electrospinning' process is a very simple and versatile process that creates nanofibers with diameters ranging from a few namometers to several micrometers through an electrically charged jet of polymer solution. This electrospinning process has been known for 70 years with the first patent issued by Formhals in 1934 [3] who was granted the first detailing an apparatus and a process for producing polymer fibers from cellulose acetate by using electrostatic force. For the past few years, polymeric nanofibers produced by electrospinning have become a topic of great interest because the electrospun has large surface area per unit mass and small pore size which can be applied into several applications. Since electrospinning is basically the drawing of polymer fluid, there are many different types of polymers and precursors that can be electrospun to form fibers. The materials to be electrospun will depend on the applications. Materials such as polymers and polymer nanofiber composites can be directly produced by electrospinning. Furthermore, a wide range of fabric properties such as strength, weight, porosity, and surface functionality can be achieved depending on the specific polymer being used. In 1996, Reneker [4] has shown the possibility to electrospin a wide range of polymer solution. The electrospinning process which has the inherent properties can form the deposit control of polymer fibers onto a target substrate, nanofibers with complex and seamless three-dimensional shape, and electrospun nanofibers can even be aligned to construct unique functional nanostructure such as nanotubes and nanowires. In the year later significant progress has been made and the resultant nanostructures have been exploited to the interesting research area of producing ceramic and composite nanofibers with various composition and properties such as carbon nanofibers made from electrospun precursor polymer nanofibers, encapsulation and alignment of carbon nanotubes within nanofibers to construct unique functional composite nanostructure, and organic-inorganic nanofibers (hybrids) [5]. Recently, there has been a growing interest in

the fabrication of nanofiber of binary metal oxide by combining the sol-gel method and the electrospinning [6-8]. Moreover, one dimensional, inorganic, nanosized fibers and fibrous mats are of interest for their high thermal stability and large surface to mass ratio. Recently, silica nanofiber mats have been produced using sol-gel synthesis/electrospinning technique without using any polymer binder by Choi.S [7]. Previuosly, the achievement of the incorporate of metal oxides into electrospun fibers has been used polymer as a binder due to its better processabilities. However, the fiber disintegration has been made by the high temperature calcination need to grow transition metal oxide crystals. If silica is used as a support for catalyst, however, the metal precursor can be added to the silica fiber by impregnation technique after calcination that SiO_4 are formed bonds.

2.1.1 Sol-gel chemistry of metal oxide to form fiber [9]

The sol-gel process, the transition of a system from a liquid (sol) into a solid (gel) phase, is a process for making ceramic and glass materials. In general the metal alkoxide such as silicon alkoxide $Si(OR)_4$ has been used as the starting materials to prepare the sol-gel. Typical sol-gel process consists of hydrolysis and condensation steps to form siloxane polymers. The hydrolysis reaction of $Si(OR)_4$ proceeds via the replacement of OR groups by OH (Eq. 2.1). Then OH groups in the hydrolysis products are active toward condensation reaction to form $\equiv$Si-O-Si$\equiv$ bonds (Eq. 2.2, 2.3)

$$Si(OR)_4 + 4H_2O \longrightarrow Si(OH)_4 + 4ROH \qquad (2.1)$$

Condensation reaction

$$\equiv Si\text{-}OR + \equiv Si\text{-}OH \longrightarrow \equiv Si\text{-}O\text{-}Si \equiv + R\text{-}OH \qquad (2.2)$$

$$\equiv Si\text{-}OH + \equiv Si\text{-}OH \longrightarrow \equiv Si\text{-}O\text{-}Si \equiv + H_2O \qquad (2.3)$$
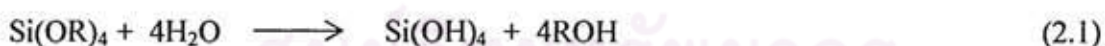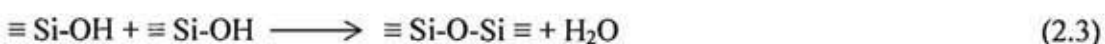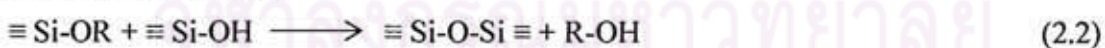
The validity of the above reaction scheme was experimentally examined for the $Si(OC_2H_5)_4(TEOS)/H_2O/C_2H_5OH/HCl$ system. For that purpose, solutions with various

compositions were prepared. All the solution were gradually increased in viscosity with reaction time and set to gels.

2.1.2 The electrospinning process

A typical electrospinning set-up consists of a high voltage power supply, a programmable syringe pump (Kd Scientific), syringe, needle, and a grounded collector screen, Fig. 2.1. The electrospinning process involves the application of a strong electrostatic field to a capillary connected with a reservoir containing a spinning solution. When a sufficiently high voltage is applied to a liquid droplet, the body of the liquid becomes charged. If the voltage surpasses a threshold value, electrostatic forces will overcome the surface tension of the droplet, and a charged liquid jet is ejected as Taylor cone (Fig 2.1). The jet is then elongated by a whipping process caused by electrostatic repulsion initiated at small bends in the fiber, until it is finally deposited on the grounded collector and a thin fiber is deposited on the counter electrode.
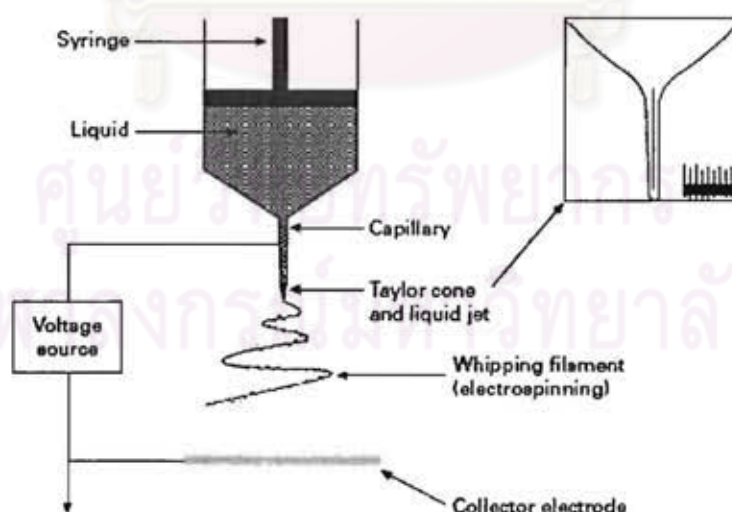
Figure 2.1 Schematic diagram of electrospinning process. [11]

Important feature of electrospinning are that firstly the polymer should be dissolved with suitable solvent. Secondly the vapor pressure of the solvent should be suitable to maintain the fiber integrity when it reached the target with the fast evaporation but not too quickly to allow the fiber to harden before it reaches the nanometer range. Thirdly the viscosity and surface tension of the solvent must neither be too large to prevent the jet from forming nor be too small to allow the polymer solution to drain freely from the syringe. Moreover the power supply should be adequate to overcome the viscosity and surface tension of the polymer solution to form and sustain the jet from the syringe. Lastly the tip to collector distances (TCD) should not be too small to create sparks between the electrodes but should be large enough for the solvent to evaporate in time for the fibers to form.

2.1.3 The electrospinning process parameters

2.1.3.1 Solution parameters

The properties of the polymer solution result in the fiber morphology.

2.1.3.1.1 Viscosity

One of the factors that affect the viscosity of the solution is the molecular weight of the polymer that represents the length of the polymer chain. Generally, when a polymer of higher molecular weight is dissolved in a solvent, its viscosity will be higher than a lower molecular weight of the same polymer solution. One of the electrospinning conditions to form fiber is that the solution must consist of the polymer with sufficient molecular weight and viscosity. During the stretching of the polymer solution, it is the entanglement of the molecule chains that prevents the electrically driven jet from breaking up to maintain a continuous solution jet. Another way to increase the viscosity of the solution is to increase the polymer concentration. Although viscosity is necessary for electrospinning, a viscosity that is too high will make it very difficult to pump the solution through the syringe needle and the solution may dries at the tip of the needle.

2.1.3.1.2 Surface tension

Surface tension is the phenomenon of the cohesive forces between liquid molecules. When the concentration of free solvent molecules is high, there is a greater tendency for the solvent molecules to congregate and adopt a spherical shape due to surface tension. A higher viscosity will means that there is greater interaction between the solvent and polymer molecule thus when the solution is stretched under the influence of the charges, the solvent molecules will tend to spread over the entangled polymer molecules thus reducing the tendency for the solvent molecules to come together under the influence of surface tension. Solvent such as ethanol has a low surface tension thus it can be added to encourage the formation of smooth fibers.

2.1.3.2 Process conditions

Another important parameter that affects the electrospinning process is a various external factors exerting on the electrospinning jet. This includes the voltage supplied, the feedrate, diameter of needle and distance between the needle tip and collector. Theses parameters have a certain influence in the fiber morphology although they are less significant than the solution parameters.

2.1.3.2.1 Voltage

The high voltage will induce the necessary charges on the solution and together with the external electric field, will initiate the electrospinning process when the electrostatic force in the solution overcomes the surface tension of the solution. Generally, both high negative or positive voltage of more than 6 kV is able to cause the solution drop at the tip of needle to distort into the shape of Taylor Cone, Fig 2.2, during jet initiation. Depending on the feedrate of the solution, a higher voltage may be required so that the Taylor Cone is stable. The columbic repulsive force in the jet will then stretch the viscoelastic solution. If the applied voltage is higher, the greater amount of charges will cause the jet to accelerate faster and more

9

volume of solution will be drawn from the tip of the needle. This may result in a smaller and less stable Taylor Cone. When the drawing of the solution to the collection plate is faster than the supply from the source, the Taylor Cone may recede into the needle.

The influence on the morphology of the fiber will be affected by the voltage supplied and the resultant electric field. The higher voltage will lead to greater stretching of the solution due to greater columbic forces in the jet as well as the stronger electric field. These have the effect of reducing the diameter of the fibers. In other hands, it was found that there is a greater tendency for beads formation [10]. The increased in beads density due to increased voltage may be result of the increased instability of the jet as the Taylor Cone recedes into the syringe needle.

Initiating Jet: 5.5 kV   Initiating Jet: 7.0 kV   Initiating Jet: 9.0 kV

7% PEO Fiber Mat: 5.5kV   7% PEO Fiber Mat: 7.0 kV   7% PEO Fiber Mat: 9.0 kV
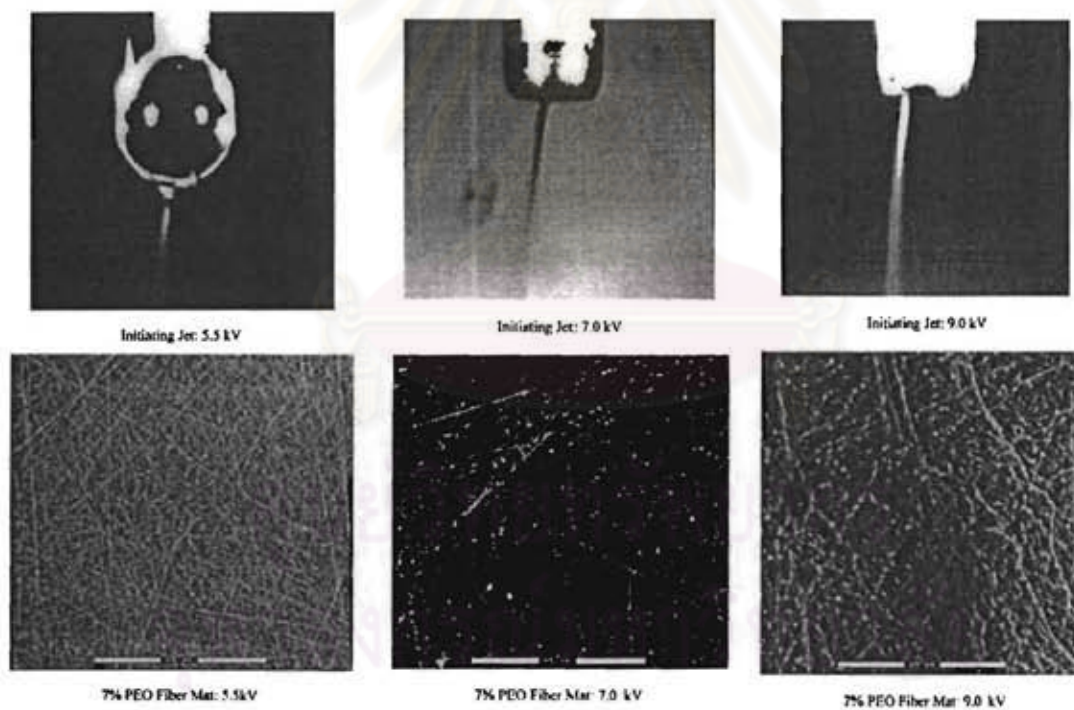
Figure 2.2 Initiating jet (top) and the corresponding fibers(bottom) produced by spinning of a 7wt%PEO/water solution at a voltage of 5.5, 7.0 and 9.0 kV (left to right). [17]

The change in fiber morphology with voltage also correlated to change the shape of the originating droplet at the capillary tip. In figure 2.2 the increasing of the applied voltage will increase the fiber bead density (bottom) and influence the solution jet origination (top) to be instable. The change in the shape of the liquid surface reflects a change in the mass balance occurring at the end of the capillary tip. Increasing the voltage causes the rate at which solution is removed from the capillary tip to exceed the rate of delivery of solution to the tip needed to maintain the conical shape of the surface. At 7.0 kV (Fig 2.2. middle) the cone has receded and the jet originates from the liquid surface within the syringe tip and moreover as the voltage of 9.0 kV (Fig 2.2. right) the jet moves around the tip edge, indicating that the jet originates on the inside of the syringe needle, where the edge of the liquid surface meets the tip wall and the fiber produced under these condition have a high density of bead defects. These phenomena showed the instability of the originating jet that affects the fiber morphology. Thus the bead formation increases with the increasing instability of the jet at the spinning tip.
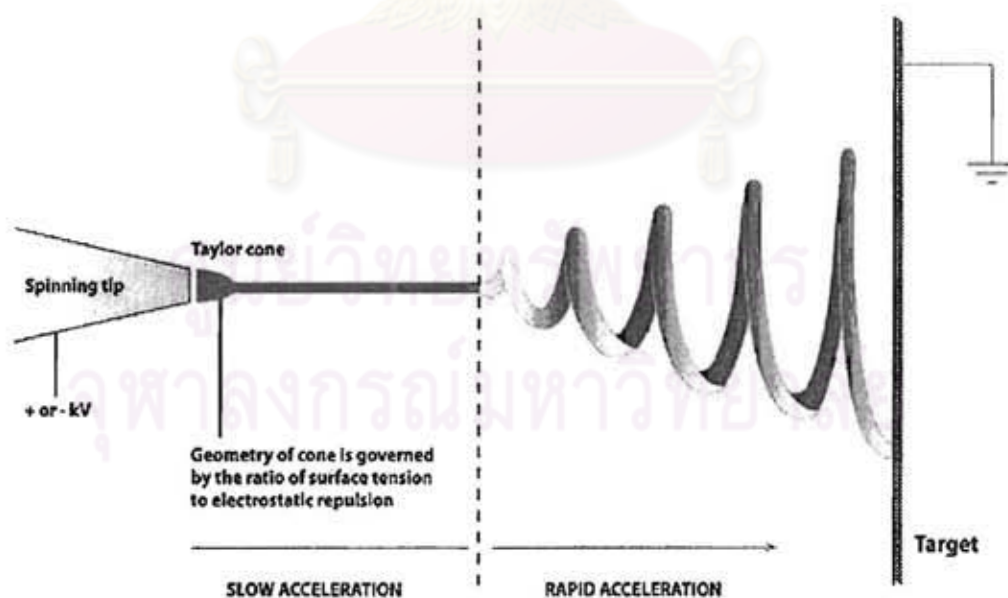
Figure 2.3 Diagram of fiber formation.

2.1.3.2.2 Feed rate

The feed rate will determine the amount of solution available for electrospinning. To maintain the Taylor Cone to be stable the adequate feedrate is necessary. When the feedrate is increased, there is a corresponding increase in the fiber diameter or beads size. A lower feedrate is more desirable as the solvent will have more time for evaporation due to the greater volume of solution drawn from the needle tip, the jet need to take a longer time to dry.

2.1.3.2.3 Diameter of needle

A small internal diameter was found to reduce the clogging as well as the amount of beads on the electrospun fibers. Decrease in the internal diameter of the orifice was also found to cause a reduction in the diameter of the electrospun fibers. When the size of droplet at the orifice is decreased, the surface tension of the droplet increases. For the same voltage supplied, a greater columbic force is required to cause jet initiation. As a result, the acceleration of the jet decreases and this allows more time for the solution to be stretched and elongated before it is collected.

2.1.3.2.4 Distance between tip and collector

Varying the distance between the tip and the collector will have direct influence in both the flight time and electric field strength. As shown in Fig 2.3 when the distance is reduced, the jet will have a shorter distance to travel before it reaches the collector plate. Moreover, the electric field strength will also increase at the same time and this will increase the acceleration of the jet to collector. As a result, there may not have enough time for solvents to evaporate when it hits the collector that may cause the fibers to form junctions resulting in inter and intra layer bonding.

2.1.4 Applications

The eventually applications of the electrospinning are multifunctional membrane, biomedical structure elements(scaffolding used in tissue engineering, wound dressing, drug delivery, artificial organs, vascular grafts), protective shields in specialty fabrics, filter media for submicron particles in separation industry, composite reinforcement, and structures for nano-electronic machines among others.[12] Thus, the emphasis of this research is to exploit the silica fiber as a support for the catalyst for steam reforming reaction.

2.2 Steam reforming of glycerol process

Steam reforming is a process used to convert a hydrocarbon-steam mixture into a mixture of (primary) H_2 and CO_2. Glycerol can be efficiently converted in hydrogen by means of its catalytic reaction with steam.

The process involved complex reactions. As a result, several intermediate byproducts are formed and end up in the product steam affecting final purity of the H_2 produced. The overall reaction for hydrogen production by steam reforming of glycerol is:

Overall reaction $\quad C_3H_8O_3 + 3H_2O \longleftrightarrow 3CO_2 + 7H_2 \ (\Delta H_o = +346.4 kJ/mol) \quad$ (2.4)

Glycerol decomposition	$C_3H_8O_3 \longleftrightarrow 3CO + 4H_2$	(2.5)
Water-Gas shift reaction	$CO + H_2O \longleftrightarrow CO_2 + H_2$	(2.6)
Steam reforming of methane	$CH_4 + H_2O \longleftrightarrow CO + 3H_2$	(2.7)
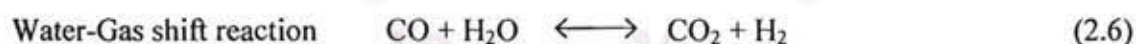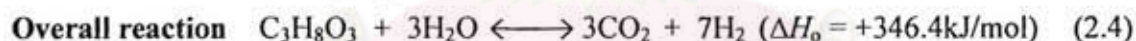
The steam reforming process can be carried out at atmospheric pressure. It is strongly endothermic (Eq.2.4), and ideal it must be carried out at high temperature and high steam to glycerin ratio to achieve higher conversion [14].

The reaction mechanism is described by Czernik [13]. Organic molecules adsorb on metal crystallite site, while water molecules are supported on the support surface. Hydrogen is produced via dehydrogenation of adsorbed organic molecules and reaction of adsorbed

organic fragments with hydroxyl groups, which migrate from the support to the metal crystallite/support interfaces. The second reaction also results in the formation of carbon oxides. The above chemical processes are accompanied by side reactions leading to the formation of carbon deposits on the catalyst surface. Pereira [28] proposed a bi-functional mechanism for alkylated aromatics selective reforming reaction, where the water is activated on the support as hydroxyl groups and the hydrocarbon to be reformed is activated by the metal particle. According to this mechanism, oxide supports with high surface mobility of hydroxyl groups would favor for steam reforming reaction.

2.2.1 The factors controlling selectivity for glycerol steam reforming

The most important parameters in the catalytic steam reforming of glycerol process are catalyst that is mainly used to increase the reaction rate and to increase the selectivity of hydrogen, feed flow rate, temperature, and water glycerol molar ratio. It is strongly endothermic, and ideally, it must be carried out at high temperature, low pressure, and high steam to glycerol ratio to achieve higher conversion [16].

2.2.1.1 Temperature

Since the steam reforming of glycerol is highly endothermic reaction (Eq. 2.6), high temperature favors glycerol conversion; therefore, the glycerol conversion increases with increasing the reaction temperature. At high temperature the methane is favorable reformed into H_2 and CO resulting in the selectivity of CH_4 decreases. The increasing temperature also has the effect of increasing H_2 selectivity could be mainly due to the CH_4 reforming process. Indeed CO selectivity should be increased when increasing the temperature but it decreases in case of excess steam because CO is reacted with H_2O in water gas shift reaction to produce CO_2 and H_2 that result the CO_2 selectivity increases as the reaction temperature increases.

2.2.1.2 Feed flow rate

The H_2 selectivity and glycerol conversion increases with a decreasing in flow rate which attribute to the increasing of the residence time. As increasing the feed flow rate, the contact time with the catalyst reduce and lower the glycerol conversion. However, with the increase in the flow rate, selectivity towards CH_4 increases. Obviously, the formation of methane in the glycerol reforming is not desirable because it reduce the selectivity toward hydrogen.

2.2.1.3 Water glycerol mole ratio

The thermodynamic analysis of the water glycerol reaction shows that at high water concentration, steam reforming of glycerol is favored. An increase in the amount of water also has the effect of increasing the extent of the water gas shift (WGS) in Eq. 2.6 and methane steam reforming in Eq. 2.7 reaction reducing undesirable products. In the WGS, carbon monoxide is reacted with steam to give CO_2 and H_2. The reaction is exothermic and independent of pressure. WGS reaction increase the H_2: CO ratio and, consequently, reduce the CO content of this gas stream. However, the reforming process consumed a considerable amount of energy with increase in water molar ratio. Too high water to glycerol ratio increasing the energy required for vaporization of water.

2.2.1.4 Catalyst

In accordance with the literature, noble metal catalysts such as Pt, Rh and Ru are active and stable for steam reforming, but their cost is the major disadvantage for using in the industrial application. For that reason Ni-based catalysts are the most used for hydrogen production in industrial scale. Nickel [3-7] was widely used in the steam reforming of methane, ethanol and glycerol because of high C-C bond-breaking activity and low cost.

The nature of support strongly influences the catalytic performance of supported Ni catalyst for steam reforming of glycerol since it effects dispersion and stability of the metal as well as it may participate in the reaction. According to the literature, the performance of the catalyst was greatly influenced by the type of supports through interactions between active metal and supports. Therefore, modification of an appreciate support for a nickel catalyst can be a feasible route to improve the catalytic performance of a catalyst and it is well known that catalyst activity can be enhanced by increasing the surface area of the catalyst per unit volume. The most common support material is porous support which typically will exert serious diffusion limitations on bulky reactants or cause pore plugging by coke. In this respect, the fiber supports which have no pore appear to be interesting candidates because of their high surface area per unit. GaO et al. [26] found that the La_2CuO_4 crystal nanofibers showed an excellent catalytic performance for steam reforming process of methanol at low temperature. Similarly Kim et al. [27] found that Pt-loaded TiO_2 nanofibers as catalyst for water gas shift reaction prepared by electrospinning precess. It was observed that their activity was 5-7 times higher than that of a bulk catalyst attributed to the larger surface area of the nanofiber.

Additionally, in several studies the addition of a second metal is investigated. Particularly the production of hydrogen by steam reforming was strongly influenced by the addition of small amount of oxygen [15, 22-23]. Zhang el al. [15] performed a glycerol steam reforming process over ceria-supported metal catalysts. Results showed that Ir/CeO_2 was no remarkable deactivation under the current operation conditions and pointed out that high oxygen storage/release capacity of CeO_2, the high dispersion and interaction of metal with support would lead to good anti-carbon deposition. Similarly, Dong et al. [22] studied the mechanism over Ni/CeO_2, Ni/ZrO_2 and $Ni/Ce-ZrO_2$ catalysts. They found that the addition of ceria to zirconia enhanced the activity of the catalyst for CH_4 dissociation and improved the carbon deposited. Due to its high oxygen storage/ release capacity which supply the oxygen to react with CO or carbon deposited changed into carbon oxide thus it has been examined as a promoter of both the activity and selectivity of the catalyst.

2.2.1.5 Catalyst characterization

2.2.1.5.1 The morphology of catalysts

The surface analysis and the diameter of fiber were determined by scanning electron microscopy (SEM)

The shape and sizes of the metal particles located on the silica surface were determined by transmission electron microscopy (TEM)

2.2.1.5.2 Crystallization properties

The X-ray diffraction (XRD) analysis was performed in order to identify the different phases present in the catalyst and to determine their crystallinity.
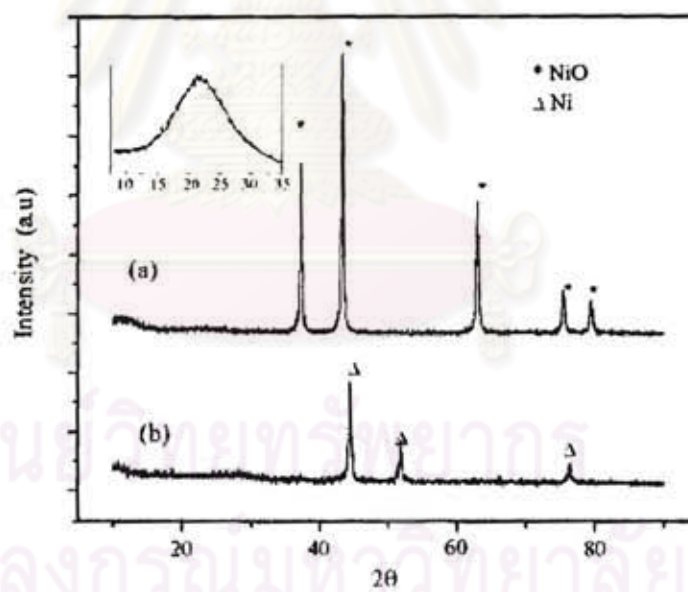
Figure 2.4 XRD patterns of Ni-SiO$_2$ nanocomposites (a) un-reduced sample and (b) reduced sample at 600°C for 4 h. [19]

The diffraction peaks of NiO in figure 2.4(a) appearing at a $2\theta = 37.5$, 43, 62, 78, and 80 assigned to the (111), (200), (220), (311), (222) planes for pure face centered cubic (fcc).

The diffraction peaks of metallic Ni in figure 2.4(b) appearing at a $2\theta =$ 44.5, 51.8 and 78.5 assigned to the (111), (200), (220) planes.

No crystalline SiO_2 phase is found because the SiO_2 is amorphous.

2.2.1.5.3 Reducible properties

The reduction behavior of the Ni species on the support was determined by temperature-programmed reduction (TPR). The TPR data showed the differences in the relative proportion of nickel species depending on the support used to disperse the nickel entities in term of the amount of H_2 consumed by the reduction of NiO in the catalyst (Eq. 2.8).

$$NiO + H_2 \longrightarrow Ni^0 + H_2O \qquad (2.8)$$
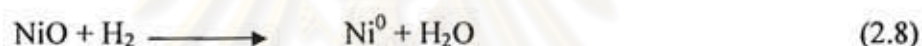
2.2.1.6 Coke formation

Generally, the catalytic activity of supported Ni catalysts decreased with time on stream due to the deposition of a large amount of carbons on the catalysts. The several reactions which are undesirable and affecting the purity of the reformation products will cause the formation of carbon, and lead to loss of effective surface area, lower the heat transfer rate from catalyst to gas, and plug of the void space within the catalyst. Zhang *et al.* [15] found that the dehydration of glycerol the ethylene or propylene, which is usually contributed to a rapid deactivation of the catalysts through coke formation, leaded to block up the catalysts pore.

The possible reactions that can be attributed to carbon formation are given as follows:

$$CH_4 \text{ (g)} \longleftrightarrow 2H_2 \text{ (g)} + C\text{(s)} \qquad (2.9)$$
$$2CO \text{ (g)} \longleftrightarrow CO_2 \text{ (g)} + C\text{(s)} \qquad (2.10)$$

$$CO(g) + 2H_2(g) \longleftrightarrow H_2O(g) + C(s) \qquad (2.11)$$

$$CO_2(g) + 2H_2(g) \longleftrightarrow 2H_2O(g) + C(s) \qquad (2.12)$$

$$C_nH_{2n} \longrightarrow {}_nC(s) + nH_2 \qquad (2.13)$$
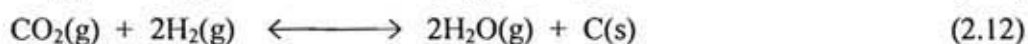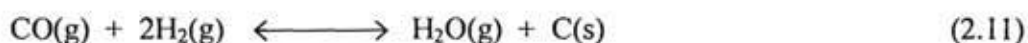
At high temperature steam cracking may occur to form alkenes that might easily form carbon (Eq. 2.13).

Figure 2.5 showed the carbon nanofibers deposited from methane decomposition (Eq. 2.9) growing with a filamentous structure. Furthermore the Ni metal particles were located at the tips of carbon nanofibers and the diameters of the carbon nanofibers were almost the same as that of the Ni particles. It is generally accepted that the surface of the Ni metal particle present on the tip of a carbon nanofiber adsorbs methane and decomposes it into carbon and hydrogen atoms to form carbon nanofibers.

(a)   (b)   (c)
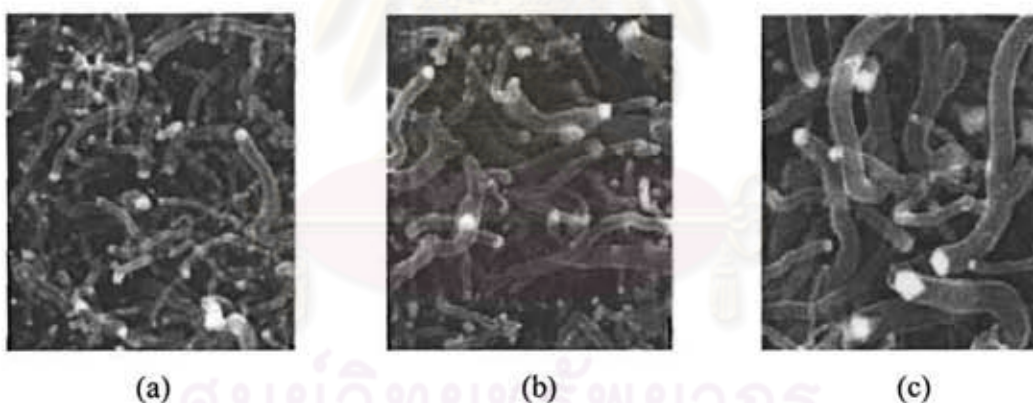
Figure 2.5 SEM images of (a) 13wt% (b) 40wt% (c) 70wt% of Ni/SiO$_2$ catalysts at the early period of methane decomposition at 773 K. [18]

Figure 2.6 revealed the different types of carbon structure formed by the methane decomposition at different temperatures. At lower temperature (773K), carbon nanofibers were formed by formation of carbon atoms from methane on the surface of Ni particles and followed by the diffusion of carbon atoms through the Ni particles. In addition, the graphene layers in the nanofiber are canted with respect to the longitudinal axis of the fibers (fish-bone

type carbon fiber), and the Ni metal particle present is pear- shape. While carbon nanotubes were found at high temperature (973K) due to the diffusion process of carbon atoms occurring on the surface of Ni metal particles was different. Moreover the carbon nanotubes with graphene layers in the nanotubes aligned along the fiber axis (multiwalled carbon nanotubes) are formed. The carbon formation reactions can be minimized by adding excess steam (Eq. 2.11 and Eq. 2.12).

(a)   (b)
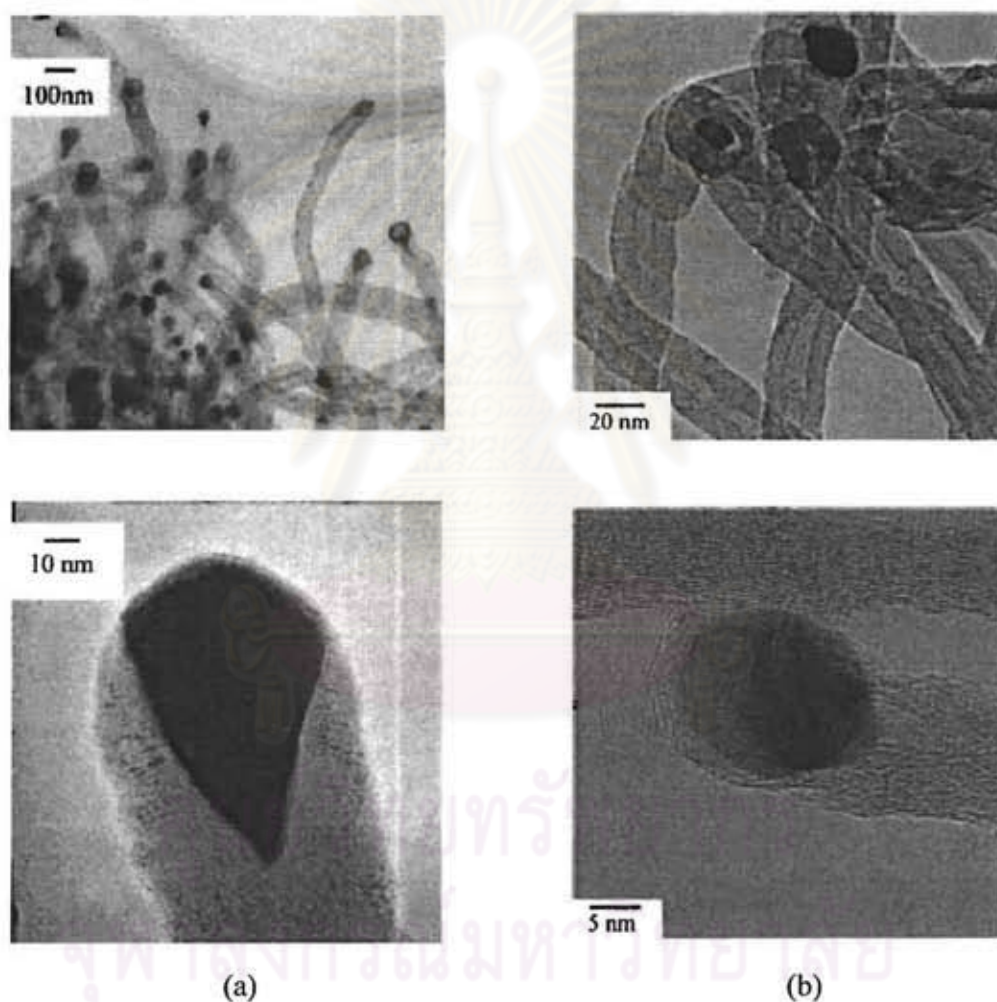
Figure 2.6 TEM images of the carbon formed by methane decomposition over 40wt%Ni/SiO$_2$ at (a) 773 K (b) 973 K. [18]

Literature reviews

In 2001, Deitzel *et al.* [17] evaluated the effects of two parameters which are spinning voltage and solution concentration on the morphology of poly(ethylene oxide) fiber produced by electrospinning process. The spinning voltage strongly affected the formation of bead defects which were increased by the increasing the spinning voltage. Solution concentration has been found to most strongly affect the fiber size, with fiber diameter increasing with increasing solution concentration.

In 2006, Joo *et al.* [8] accomplished with the incorporation of V_2O_5 into silica nanofibers which were produced by coaxial electrospinning a silica sol-gel precursor containing vanadium oxytriisopropoxide (VOTIP) followed by calcination at high temperatures, and the effect of the addition of V_2O_5 on the properties of fiber was studied. SEM images showed the inorganic hybrid fibers are submicron in diameter, and the additional 23mol% of vanadium is the smallest fiber of 510 ± 220 nm in average diameter after calcined at $800^{\circ}C$ for 6 hr. The physisorption experimental reveal that silica nanofibers have a high specific surface area of 63 m^2/g. EFTEM images show the growth of vanadium crystals on the surface of fiber after calcinations. The increasing concentration of vanadium increase the rate of gelation and sol-gel will be spinnable at earlier and shorter of time period.

In 2007, Lee *et al.* [6] studied the direct formation of silica/titania composite nanofiber without any gelator or binder using sol-gel method and electrospinning technique using tetraethyl orthosilicate (TEOS) and titanium(IV)isopropoxide (TiP) as a sol-gel precursor followed by calcination. The diameter of composite fiber submicrometer was analyzed by SEM. The crystallization and surface morphology of electrospun fiber are influenced by the calcinations temperature and titania loading content. XRD results shown that the anatase phase in composite fibers can be preserved even after high temperature processing at lower content of titania.

In 2007, Zhang *et al.* [15] studied the steam reforming of ethanol and glycerol using Ir, Co and Ni supported on ceria as catalyst prepared by co-precipitation technique. Ir/CeO_2 was significantly active and selective for hydrogen production. To investigate the reaction pathway at temperature below $350^{\circ}C$ the main gas products (acetaldehyde acetone and methane) were found due to dehydrogenation and decarbonylation reaction, and the much lower concentration of CO was converted in to CO_2 indicated that the water gas shift reaction took place. The reaction pathways of ethanol steam reforming at low temperature is strongly by dependent on the capacity of the active metals for breaking the C-C bond in ethanol molecule. However the concentrations of acetaldehyde and acetone decreased rapidly with increasing temperature above $350^{\circ}C$ at which H_2 CO_2 CH_4 and CO became the main products. At temperature above $500^{\circ}C$ a rapid decrease of methane resulted by steam reforming of methane. Additionally the steam reforming of glycerol using Ir/CeO_2 catalyst at $400^{\circ}C$ exhibited the complete conversion of glycerol and more than 85% .selectivity of hydrogen. According to redox properties of CeO_2 which has the very fast reduction of $Ce^{4+}Ce^{3+}$ associated with the formation of vacancies at the surface and the water molecule was activated by cerium dioxide with high OH groups at the surface mobility. The reaction of the intermediate activated by metal with OH groups generated on the surface of ceria primarily led to the formation of CO and methane. Meanwhile, the much lower concentrations of CO could be attributed to the water gas shift reaction promoted by the high OH group surface mobility of CeO_2.

In 2008, Adhikari *et al.* [16] studied the effect of different kind of supports such as CeO_2, MgO and TiO_2 on the steam reforming process over nickel catalysts prepared by incipient wetness impregnation method. The specific surface area and metal dispersion of Ni/CeO_2 were 67.0 m^2/g and 6.14%, respectively due to the better interaction of CeO_2 with nickel precursor. For steam reforming reaction the effect of condition parameters such as reaction temperature, feed flow rate (FFRs), and water/glycerol molar ratios (WGMRs) on hydrogen selectivity and glycerol conversion were investigated. Ni/CeO_2 was found the best catalyst that gave maximum hydrogen selectivity of 74.7% at a WGMR of 12:1, temperature of $600^{\circ}C$, and FFR of 0.5 mL/min compared to Ni/MgO (38.6%) and Ni/TiO_2 (28.3%) under

the same conditions. When increased the reaction temperature glycerol conversion and hydrogen selectivity were increased due to the CH_4 reforming process that is the endothermic reaction. However the conversion of glycerol and selectivity of hydrogen were decreased by mean of increasing the feed flow rate due to the contact time with the catalyst reduced. The increasing of WGMRs increased hydrogen selectivity significantly.

In 2008, GaO *et al*. [26] studied the new kind of catalyst for steam reforming of methanol as La_2CuO_4 nanofibers prepared by using single-walled carbon nanotubes as templates under mild hydrothermal conditions. The La_2CuO_4 nanofibers completely converted methanol into H_2 and CO_2 with no CO production at low temperature ($150^{\circ}C$). There was no significant drop in activity within 60 h reaction test on stream when compared to La_2CuO_4 bulk powder. The nanofiber has high specific surface area ($105 \ m^2/g$).

CHAPTER III

EXPERIMENTAL

3.1 Materials

All chemicals used in this experiment were listed in table 3.1.

Table 3.1 List of chemicals and sources

Chemicals	Source
Tetraethyl orthosilicate ($C_8H_{20}O_4Si$) 98.0%	Fluka
Hydrochloric acid 37.0%	CARLO ERBA
Ethanol 99.8%	Analar Nor Mapur
Nickel acetate $(CH_3COO)_2Ni.4H_2O$ 99.0%	Unilab
Cerium acetate $(C_2H_3O_2)_3Ce.xH_2O$ 99.9%	Aldrich
Glycerol ($C_3H_8O_3$) 99.5%	Univar
Silica supports 5-10 mesh	Fuji Silysia
Nitrogen gas (99.99% purity)	Praxair
Hydrogen gas (99.99% purity)	Praxair
Standard synthesis gas 1% of $H_2/CO/CO_2/CH_4/C_2H_4/C_2H_6$ bal N_2	BOC scientific

3.2 Instruments and Equipments

3.2.1 Instruments and Equipment for Catalyst Preparation

1. High voltage power supply
2. Syringe pump
3. Ultrasonic bath
4. Water bath
5. Mechanical stirrer and impeller
6. Hot plate

7. Pipette 1, 5 and 10 mL

8. Magnetic stirrer

9. Disposal syringe

10. Thermometer

11. Aluminium foil

12. Stainless steel screen 20 x 20 cm

13. Dessicator

14. Oven

15. Balance 4 decimal system

16. Crucible

17. Beaker 50 and 250 mL

3.2.2 Instruments and Equipment for Catalyst Characterization

1. X-ray diffractometer (XRD) (Philips model X'Pert)

2. Scanning electron microscope (SEM) (JOEL model JSM-6480LV)

3. Energy dispersive spectroscope (EDS)

4. Temperature programmed reduction (TPR)

5. Transmission electron microscope (TEM)

6. Thermal gravity analysis (TGA)

3.2.3 Instruments and Equipment for Glycerol Steam Reforming Process

1. Quartz tube reactor

2. Mass flow controller (KOFLOC)

3. Syringe pump (New Era Pump System)

4. Evaporator

5. Thermocouple

6. Tube furnace and temperature controller

7. Cooled trap

8. Gas bag
9. Gas Chromatography (GC) (Shimadzu GC-2014)

3.3 Preparation and characterization of catalyst

3.3.1 Sol-Gel preparation

The silica sol was prepared from tetraethyl orthosilicate (TEOS), distilled water, ethanol, and HCl. The molar ratio of TEOS:Ethanol:H_2O:HCl was 1:2:2:0.01. The sol was prepared as follows. Firstly, TEOS was mixed with distilled water in a beaker under vigorous stirring. Then, HCl and ethanol were added to the solution. Finally, the solution was heated at 55^oC for 50 min and cooled down to room temperature.

3.3.2 Electrospinning process

The electrospinning process was presented in figure 3.1. The sol was placed in the disposable syringe with 0.6 mm diameter needle and an electrode was directly connected with the solution. The applied voltage was 15 kV and the tip-to-collector distance was 15 cm. The fibers were placed in a convention oven at 110^oC for overnight to evaporate the remaining solvents. The solvent-evaporated fibers were calcined at 500^oC for 2 h.
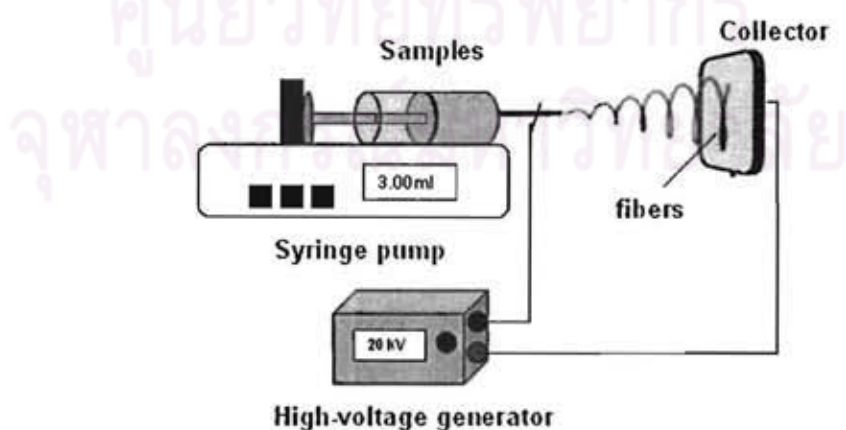
Figure 3.1 The electrospinning process apparatus.

3.3.3 The influence of the parameters on the electrospinning process

The effect of the parameters on the fiber diameter and morphology were investigated, and were listed as follows:

      1. The effect of voltage (15, 20 and 25 kV)

      2. The effect of tip to collector distance (10, 15 and 20 cm)

3.3.4 Impregnation

The calcined silica fiber was impregnated with nickel acetate solution, and the percentage of nickel loading was investigated by 5, 10 and 20 percent by weight. Then the impregnated fiber was calcined at $500^{\circ}C$ for 2 h.

3.3.5 Characterization of As-spun fiber

3.3.5.1 X-Ray diffraction (XRD)

Structure and crystallite size measurement was performed using a Philips model X'Pert X-ray diffractometer by using $CuK\alpha$ radiation at an angle of 2θ ranged from 20 to 85 degrees.

Determination of nickel oxide crystallite size evaluated from the full half width at a half maximum of NiO XRD peak by using Scherrer equation as follow [29]:

$$\text{Crystalline size (nm)} = \frac{K\lambda}{B_{\frac{1}{2}}\cos\theta_B}$$

Where K is a unit cell geometry dependent constant

    λ is wavelength of the x-ray (0.1542 nm)

    $B_{\frac{1}{2}}$ is the full-width-half-max of the peak

    θ_B is the Bragg angle

3.3.5.2 Scanning Electron Microscopy (SEM)

To investigate morphology and diameter of the obtained as-spun fiber, a scanning electron microscope (SEM) JOEL model JSM-6480LV was used. EDS determined the composition of fiber. The size of the as-spun fiber was determined using a SemAfore program.

3.3.5.3 Thermal Gravity Analysis (TGA)

To determine the coke content of the catalysts, a PerkinElmer model PYRIS DIAMOND thermo-gravimetric analyzer was used. Sample was heated from room temperature to 850°C with heating rate 15°C/min in a flow of 50 mL/min of air.

3.3.5.3 Temperature Program Reduction (TPR)

The temperature program reduction was performed to determine the reducibility of the catalysts. The Micromeritics AutoChem II 2920 was used. The preparation was performed by flowing a Ar 50 mL/min over 60 mg of calcined catalyst, heat from ambient temperature to 100°C, kept for 1 h to remove the adsorbed water and other contaminants followed by cooling to 50°C and kept for 30 min. The reducing gas containing $10\%H_2$ in Ar was passed over the calcined catalyst at a flow rate of 50 mL/min with the heating rate of 10°C/min up to 600°C as shown in figure 3.2.

Determination of percentage of nickel reduction of catalyst was calculated as follows:

$$\text{Reduction degree (\%)} = 100 \ \times \ \frac{\text{mole of } H_2 \text{ consumption}_{measured}}{\text{mole of } H_2 \text{ consumption}_{calculated}}$$
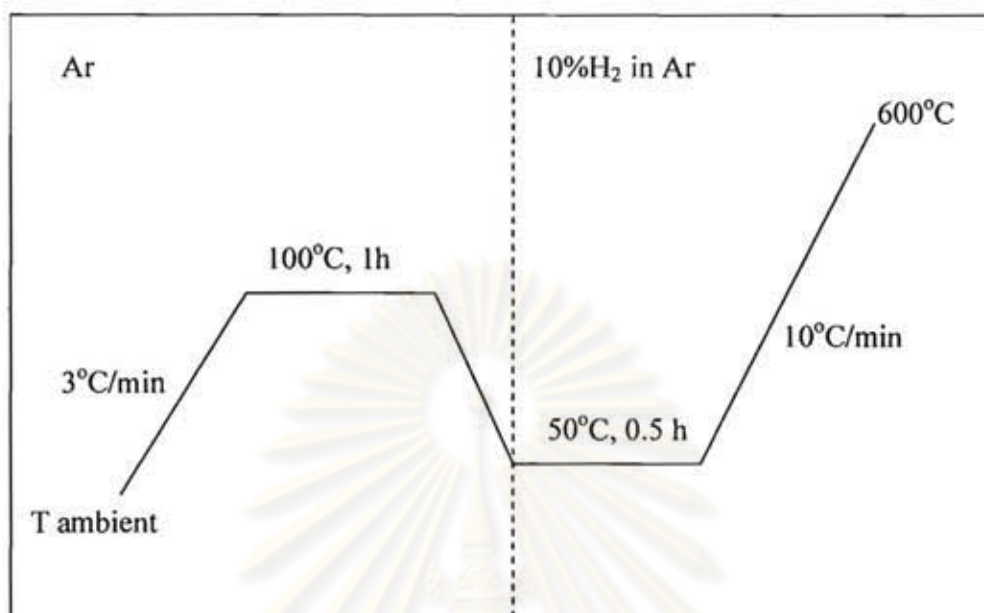
Figure 3.2 Schematic of temperature program reduction reaction.

3.4 Steam reforming of glycerol using Ni/SiO₂ fiber as catalyst.
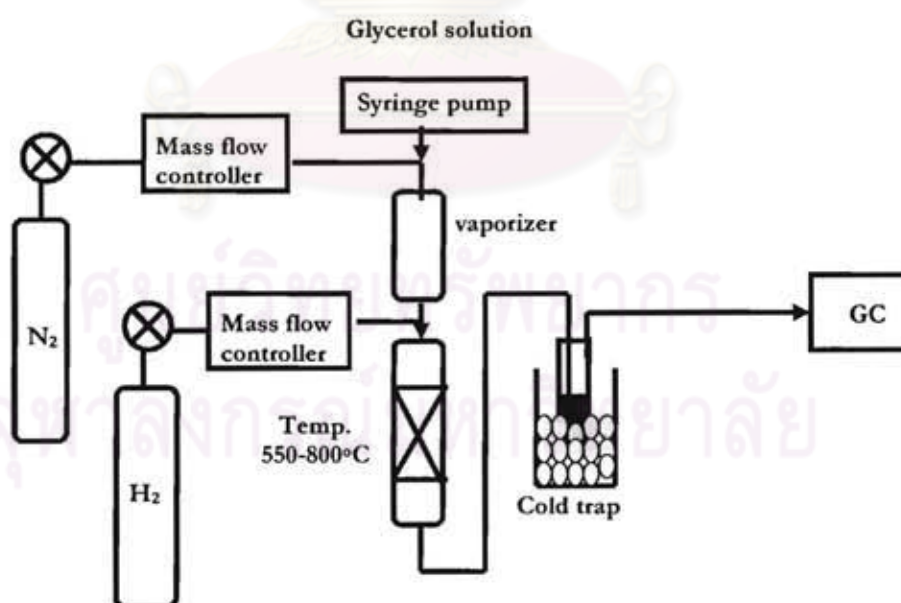
Figure 3.3 Flow diagram of glycerol steam reforming process.

3.4.1 Experimental procedure before the reaction

1. The 0.1 g of nickel/silica fiber catalyst was packed into the middle of the fixed bed quartz reactor.

2. Set temperature of tubular furnace at 700°C for reduction of catalyst with hydrogen (30 mL/min) under atmospheric pressure for 1 hour and then switched into nitrogen (10 mL/min).

3.4.2 Reaction procedure

1. Set up reaction temperature of tubular furnace for the reaction.

2. Glycerol solution was continuously fed by syringe pump into the evaporizer setting temperature at 300°C that the glycerol solution were vaporized completely.

3. After 2 h of the reaction, the sampling gas was analyzed by gas chromatography of which the optimum condition was showed in table 3.2.

Table 3.2 The optimum condition of gas chromatograph

Carrier gas	Ar 99.999%
Column	Unibead C
Injector temperature	120°C
Column temperature	Temperature program 50°C 3min 180°C (15°C/min) 180°C 8 min
Detector temperature	180°C
Detector	Thermal conduct detector(TCD)

3.5 The influence of the operating parameters on the performance of reaction

In this part, the effect of the operating parameters on the glycerol conversion and the selectivity were investigated. The parameters were listed as follows:

1. The effect of support (fiber and porous)
2. The effect of temperature (550 650 and 750°C)
3. The effect of feed flow rate (0.01 0.03 and 0.05 mL/min)
4. The effect of water/glycerol mole ratio (3:1 6:1 and 9:1)
5. The effect of nickel loading (5 10 and 20 wt %)
6. The effect of additional cerium (1 and 2 wt %)

3.6 Analysis of the reaction products

The effluent gases were analyzed by a Shimadzu GC-2014 gas chromatography.

Determination of H_2, CO_2, CO, CH_4, C_2H_4 and C_2H_6 selectivity and glycerol conversion were calculated as follows:

$$H_2 \text{ selectivity (\%)} = \frac{H_2 \text{ mole produced}}{C \text{ atoms in gas product}} \times \frac{1}{RR} \times 100$$

Where RR is H_2/CO_2 reforming ratio = 7/3 [16] in case of complete reforming process

$$\text{Selectivity of } i \text{ (\%)} = \frac{C \text{ atoms in species } i}{C \text{ atoms produced in gas phase}} \times 100$$

Where species i = CO, CO_2, CH_4, C_2H_6 and C_2H_4

$$\text{Glycerol conversion (\%)} = \frac{C \text{ atoms in gas phase}}{\text{Total C atoms in the feedstock}} \times 100 \quad [16]$$

CHAPTER IV

RESULTS AND DISCUSSION

4.1. Catalyst preparation

4.1.1 The effect of applied voltage on the morphology of fiber in electrospinning Process

The effect of applied voltage on morphology appearance of the electrospun silica fiber was investigated. The collector distance was fixed at 15 cm. SEM images of the electrospun silica fibers at three different applied voltages 15, 20 and 25 kV was shown in figure 4.1. The fibers are submicron in diameter, and the average diameter of all fiber after calcinations at 500°C for 2 h showed in table 4.1. The electrospun obtained by 15 and 20 kV was almost the same size in diameter but different in the distribution of the fiber size as can be seen in figure 4.1(a) and 4.1(b). From figure 4.1(a) showed that the fiber obtained by 15 kV was equivalent in diameter. When increased the voltage to 20 kV a little change in the fiber distribution was found. When further increased to 25 kV the smallest average diameter of 0.93 μm and the wide range of fiber size distribution were found. This can be attributed to the instability of the jet initiate when increasing the applied voltage because of which will cause the jet to have greater amount of charge resulting in the drawing of the solution to the collection plate is faster than the supply from the source. Thus the Taylor Cone may recede into the needle resulting in the initiated jet become smaller and less stable. As a result, the collecting fiber will be small and has a wide range of fiber distribution owing to the instability.
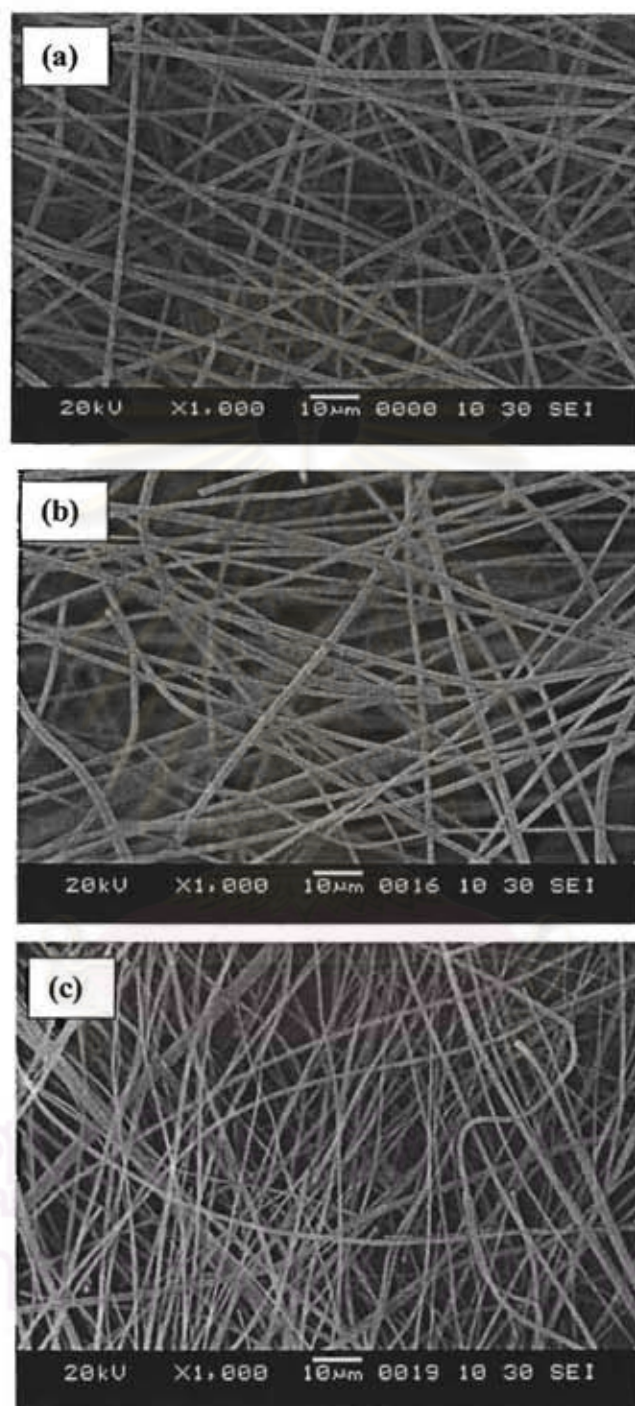
Figure 4.1 SEM images of SiO₂ fibers with various applied voltages (a) 15kV (b) 20kV

(c) 25kV. The tip to collector distance was 15 cm. The fiber was calcined

at 500°C for 2 h.

4.1.2 The effect of the tip to collector distance (TCD) on the morphology of fiber in electrospinning process

The effect of tip to collector distance (TCD) on morphology appearance of the electrospun silica fiber was investigated. The voltage was fixed at 15 kV. SEM images of the electrospun silica fibers at three different TCD, 10, 15 and 20 cm was shown in figure 4.2(a) (b) and (c), respectively. SEM image showed the fibers are submicron in diameter, and the average diameter of all fibers after calcination at 500°C for 2 h was shown in table 4.1. The electrospun obtained by 10 and 25 cm was larger than those obtained at 15 cm. This can be attributed to the electrospinning process with 15 kV and TCD of 15 cm was the appropriate condition to produce the smallest fiber in this experiment. The average fiber diameter obtained by 15 cm was 1.28 μm. When the distance was reduced to 10 cm the jet would have a shorter distance to expand before it reaches the collector plate leading to the large fiber. Moreover, the electric field strength would also increase at the same time and this will increase the acceleration, the rate of the jet drawing the solution to the collector. Thus it may not have enough time for solvent evaporation leading to the larger size of fiber obtained. In addition the distance is increased to 20 cm leading to the electric field strength decreasing and this decreases the acceleration of the jet to collector thus the fiber was large.
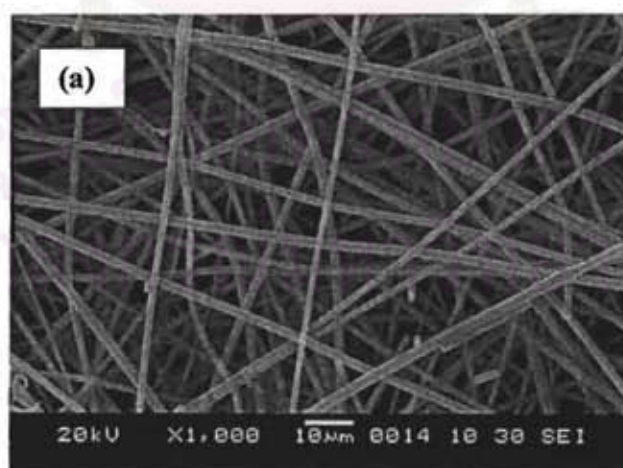
Figure 4.2 SEM images of SiO_2 fibers with various TCD (a) 10 cm (b) 15 cm (c) 20 cm. The applied voltage was 15 kV. The fiber was calcined at 500°C for 2 h.
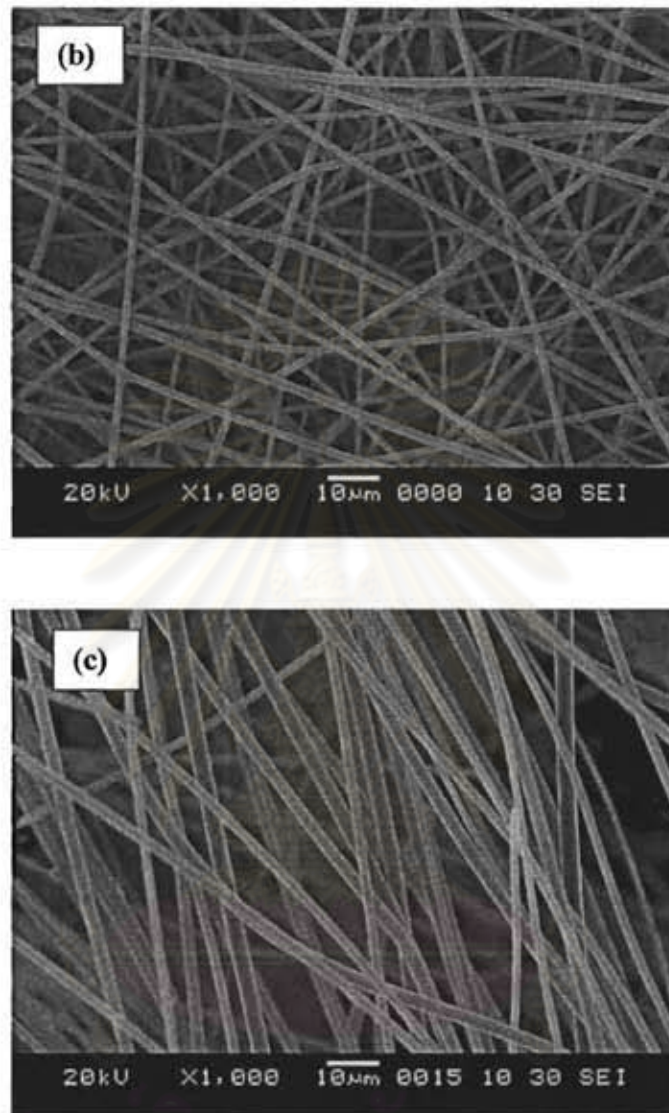
Figure 4.2 SEM images of SiO$_2$ fibers with various TCD (a) 10 cm (b) 15 cm (c) 20 cm.
The applied voltage was 15 kV. The fiber was calcined at 500 ^{o}C for 2 h.
(continue)

Table 4.1 Average diameters of the SiO_2 fiber with various voltage operations (μm)

Voltage	Tip to collector distance (cm)		
(kV)	10	15	20
15	1.54±0.3	1.28±0.2	2.2±0.5
20	N/A	1.27±0.3	N/A
25	N/A	0.93±0.2	N/A

The comparison of surface area between porous silica and silica fiber was shown in table 4.2. In case of porous silica the surface area was investigated by BET method whereas the mathematic calculation from the SEM picture was used to investigate the surface area of the fiber due to the silica in the fiber form could not be analyzed by BET method (figure 4.4) because it has no pore thus the adsorption and desorption properties could not be verified. From table 4.2 the BET result showed that the porous silica has the surface area of 237.36 m^2/g and the surface area of 1.49 m^2/g was obtained from the fiber support which was prepared by 15kV and 15 cm.

Figure 4.3 showed the adsorption isotherm of the mesoporous silica. The figure showed that the adsorption isotherm type V in which the hysteresis loop was generated by the capillary condensation of the adsorbate in the mesopores of the silica solid represented the monolayer and multilayer adsorption plus capillary condensation properties[19].

Table 4.2 The surface area of silica porous and fiber

BET Result	Porous	Fiber (Mathematic calculation*)
Surface area (m^2/g)	237.36	1.49
Pore volume (cm^3/g)	1.01	N/A
Pore size (nm)	16.9	N/A

* Surface area = $2\pi r.L$

Figure 4.3 The N_2 adsorption isotherm of silica porous support.
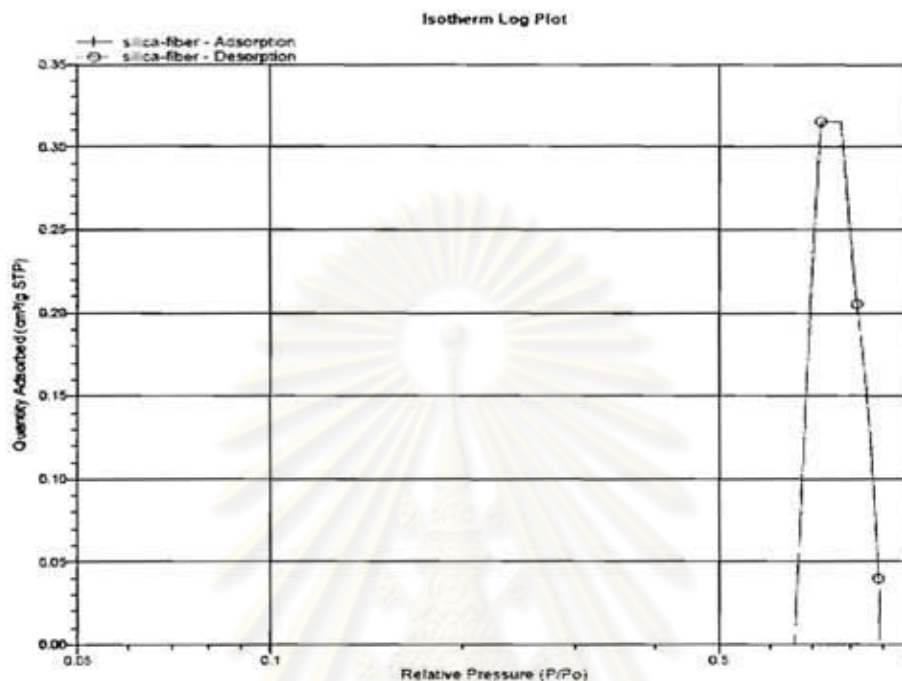
Figure 4.4 The N_2 adsorption isotherm of silica fiber support.

4.1.3. The effect of nickel loading

The electrospun fibers with various compositions of nickel/silica were prepared by impregnation technique of silica fibers, obtained by the applied voltage of 15 kV and TCD of 15 cm, with the nickel acetate solution and then calcined at 500°C for 2 h. The morphology of nickel/silica fibers analyzed by SEM at the 70,000 times magnification was investigated. The SEM images of silica fiber containing 5, 10 and 20 wt%Ni/SiO_2 after calcination are showed in figure 4.5(b), (c) and (d), respectively. The image showed the surface of the nickel/silica fiber was rougher than the surface of pure silica fiber because the Ni particles were dispersed over the fibers support. The surface of the higher concentration of nickel was clearly rougher than lower concentration. This can be attributed to the nickel particle of the higher nickel content was larger than the lower nickel content. Moreover in figure 4.5(b), the 20 weight percentage impregnated with silica fiber, the agglomeration into particle was observed.
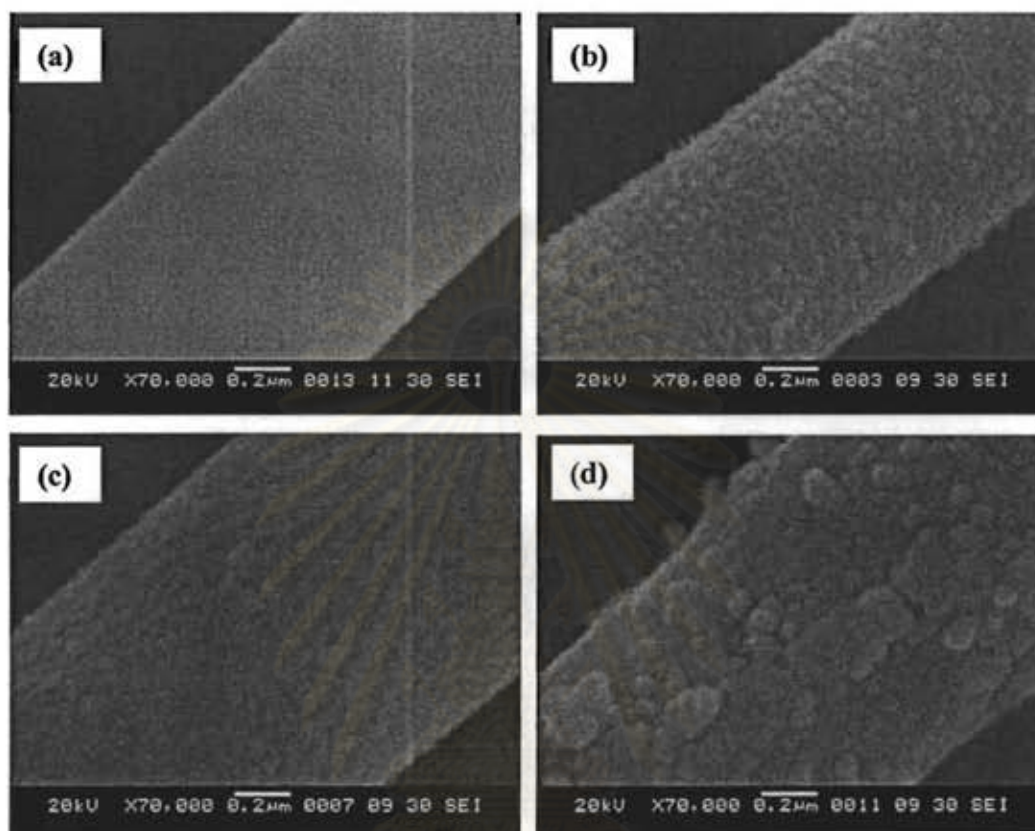
Figure 4.5 SEM images of (a) SiO_2 fibers (b) $5\%Ni/SiO_2$ fibers (c) $10\%Ni/SiO_2$
fibers (d) $20\%Ni/SiO_2$ fibers. The fiber was calcined at 500^oC for 2 h.

An energy dispersive spectroscopy (EDS) was used for evaluation the elemental compositions of fiber of 5, 10 and 20 wt% Ni/SiO_2, respectively. The results in table 4.3 showed the nickel content from the EDS analysis compared with the nickel content expected by the preparation. The result showed that the preparation of 5 and 10 wt%Ni/SiO_2 has the actual content of nickel deposited onto the fiber support of 4.53 and 9.35 wt%, respectively. For the higher nickel loading the EDS showed the 20wt%Ni/SiO_2 only contains the nickel content of 14.42 %wt. probably due to the fibers which are submicron in diameter did not have the surface area enough to support the nickel content at high level.

Table 4.3 Elemental compositions of electrospun fiber

%Ni	EDS Analysis
5	4.53
10	9.35
20	14.42
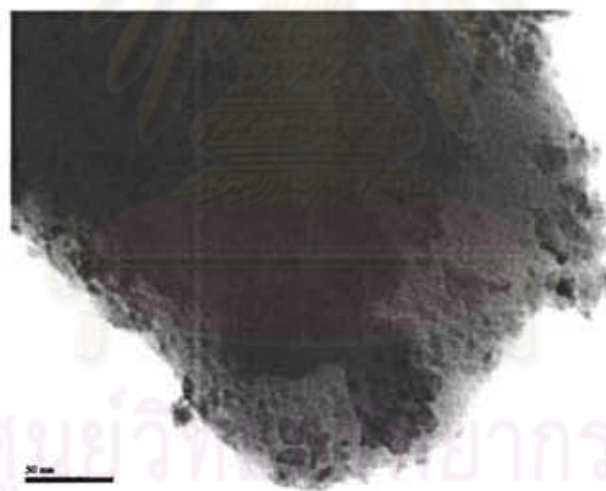
Figure 4.6 TEM image of 10wt%Ni/SiO$_2$ fiber after calcined at 500°C for 2h.

TEM image of the 10wt%Ni/SiO$_2$ fiber was shown in figure 4.6 and serve to illustrate the surface morphology/dispersion of the metal phase on the fiber support. The figure 4.6 provided clear evidence of nickel phase associated with SiO$_2$ appearing to be spherical shapes. It can be clearly seen that large particles were presented. Furthermore, the agglomeration of metal particles is clearly visible in this catalyst.
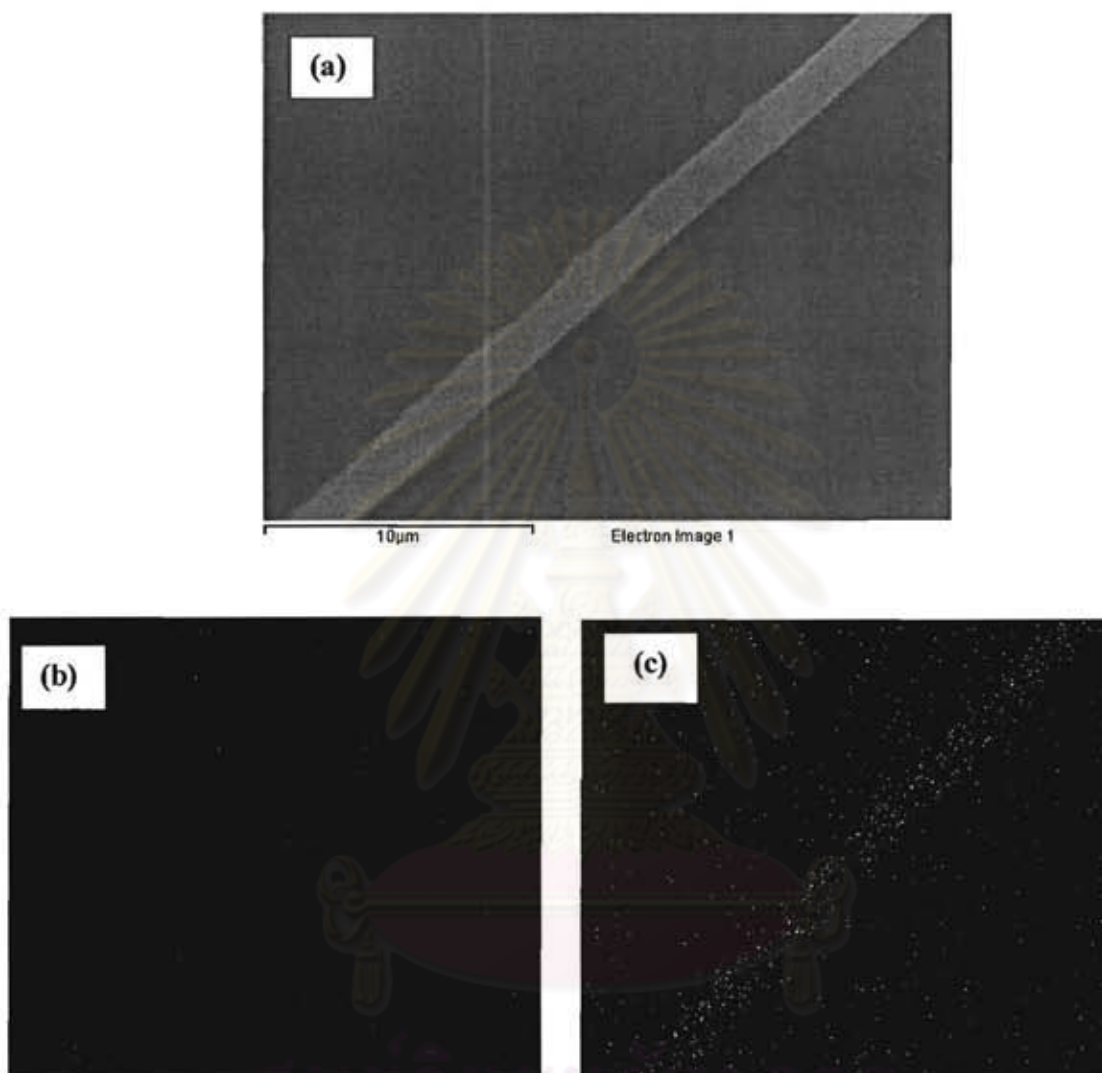
Figure 4.7 EDS mappings of (a) 20%Ni/SiO$_2$ fiber (b) the distribution of Si element
(c) the distribution of Ni element.

Figure 4.7 revealed the EDS mapping analysis indicating the distribution of the fibrous element of Si and Ni of 20wt%Ni/SiO$_2$ fiber as can be seen in figure 4.7(b) and (c), respectively. The result showed that the Ni particles were well dispersed on the silica fiber support.

4.1.4 Crystallization of Ni/SiO₂ catalyst

The X-ray diffractograms of NiO derived from nickel acetate were measured. Figure 4.8 showed diffractogram of NiO calcined at $500^{\circ}C$ for 2 h of the catalyst with different nickel loading. The XRD patterns show several diffraction peaks assigning to the (111), (200), (220), (311) and (222) plans for pure face centered cubic (fcc) NiO nanocrystals. In case of silica fiber no diffraction peaks in the XRD profiles were observed except broad halo of SiO_2 appearing at $2\theta = 26$, which indicates that the SiO_2 is in amorphous state. The XRD diffraction results indicate that the products by calcination of catalyst are composed of NiO and amorphous silica. The intensity of diffraction lines related to NiO phase increased progressively by increasing the amount of NiO loaded on the silica. The NiO peaks of 20wt%Ni/SiO₂ were sharper than the NiO peaks of the lower concentration meaning that the high nickel loading has the large NiO crystalline and was not well dispersed on silica (see figure 4.5(d)). This was attributed to the fact that for high NiO containing catalysts, a multilayer of NiO phases has been developed at the surface causing the larger NiO crystalline leading to the intensity of diffraction peaks increased. This indicated that the dispersion of nickel oxide species available for the catalyzed reaction is higher on silica-supported catalyst than lower amount of NiO.

The XRD patterns of the different cerium loading by consecutive impregnation showed in figure 4.8(f) and (g). For 1wt%Ce-10wt%Ni/SiO₂ and 2wt%Ce-10wt%Ni/SiO₂ catalysts, the XRD patterns indicated the NiO crystalline with no diffraction peaks assigned to CeO_2 and the intensity of peaks corresponding to NiO was not different from 10%Ni/SiO₂.

The crystallite size was illustrated in table 4.4 calculated based on the line width of the (200) diffraction plane, the crystallite size of NiO was determined by using Scherrer formula. The peaks corresponding to NiO intensified with an increasing in nickel loading suggesting that at low nickel loading NiO was presented in the form of small particles while at higher Ni content bulk NiO was presented by agglomeration. The additional cerium in 10%Ni/SiO₂ did not affect to the crystallite size of NiO
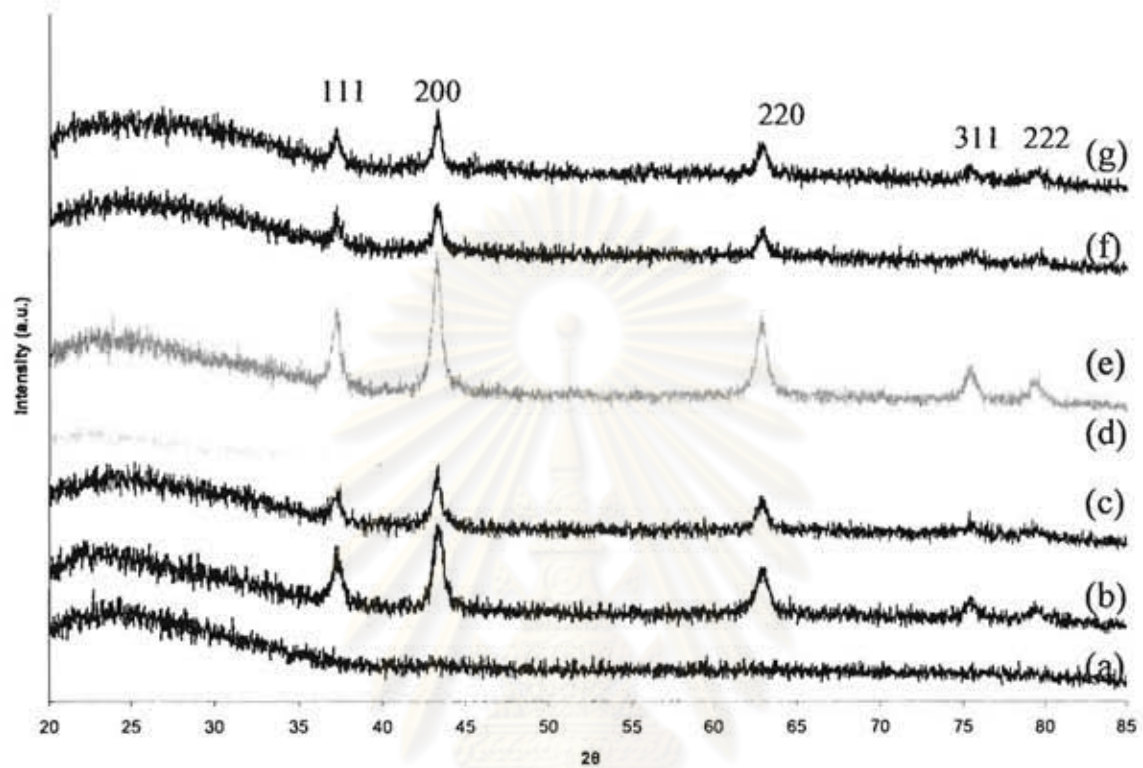
Figure 4.8 XRD patterns of (a) SiO_2 (b) 10wt%Ni/SiO_2 porous (c) 5wt%Ni/SiO_2 (d) 10wt%Ni/SiO_2 (e) 20wt% Ni/SiO_2 (f) 1wt%Ce-10wt% Ni/SiO_2 (g) 2wt%Ce-10wt% Ni/SiO_2

Table 4.4 The average particle size of difference nickel loading

%Metal loading	Crystallite size (nm)
5wt%Ni	11.31
10wt%Ni	11.37
20wt%Ni	13.95
1wt%Ce-10wt%Ni	11.31
2wt%Ce-10wt%Ni	11.31
10wt%Ni porous	10.39

4.1.5. Reducible properties of Ni/SiO$_2$ catalyst

The TPR profiles of Ni/SiO$_2$ fiber catalyst with various Ni loading (5-20wt%) compared with the 10wt%Ni/SiO$_2$ porous catalyst are shown in figure 4.9. The NiO of porous support showed two reduction peaks at 346 and 435°C while the fiber catalyst with the same nickel loading showed two peaks of reduction at 271°C and 434°C whereas the first peak was shifted to lower temperature and the intensity of second reduction peak which appeared at high temperature was low. This indicated that the fiber catalyst can be reduced easily than the porous catalyst and it mainly contained the bulk NiO phase. According to the literature, the reduction peak at low temperature is attributed to reduction of the large NiO species with small interaction with silica support, while the reduction peak at higher temperatures is related to the reduction of the NiO which has a stronger interaction with the support [3]. With an increasing in the metal loading from 5% to 10%, the intensity of the peak at low temperature increased significantly due to increasing NiO content. At a metal loading of 20wt%, only one sharp broad peak was observed. This is attributed to agglomerated NiO.

For 1wt%Ce-10wt%Ni/SiO$_2$ and 2%Ce-10wt%Ni/SiO$_2$, The TPR profiles showed a broad peak at 312 and 311°C, respectively. This broad peaks shifted to higher temperature compared with 10wt%Ni/SiO$_2$ that means a strong interaction between Ni and support. This indicated the CeO$_2$ facilitates the NiO to strongly interact with the support.

The degree of reduction was calculated from the H$_2$ consumption was shown in table 4.5. It can be clearly observed that the NiO in all catalysts were not reduced completely. For 5wt%Ni/SiO$_2$ the percentage of nickel reduction was lower than 10wt%Ni/SiO$_2$. The lower value of nickel reduction suggests that the lower percentage of nickel loading leads to the small particle size of nickel therefore the interaction between the metal and support was stronger than the high metal loading [20]. On the same support with an increasing in nickel loading from 10 to 20 wt%, the reduction degree was decreased from 95% to 67% due to the nickel particle size of 20wt% was large by the agglomeration leading to difficult reduction.

In case of 10wt%Ni/SiO₂ which was added with cerium we found that the degree of reduction was decreased with increasing the percentage of cerium. This indicated that the addition of CeO₂ facilitated the reducible properties of Ni/SiO₂ fiber catalyst.
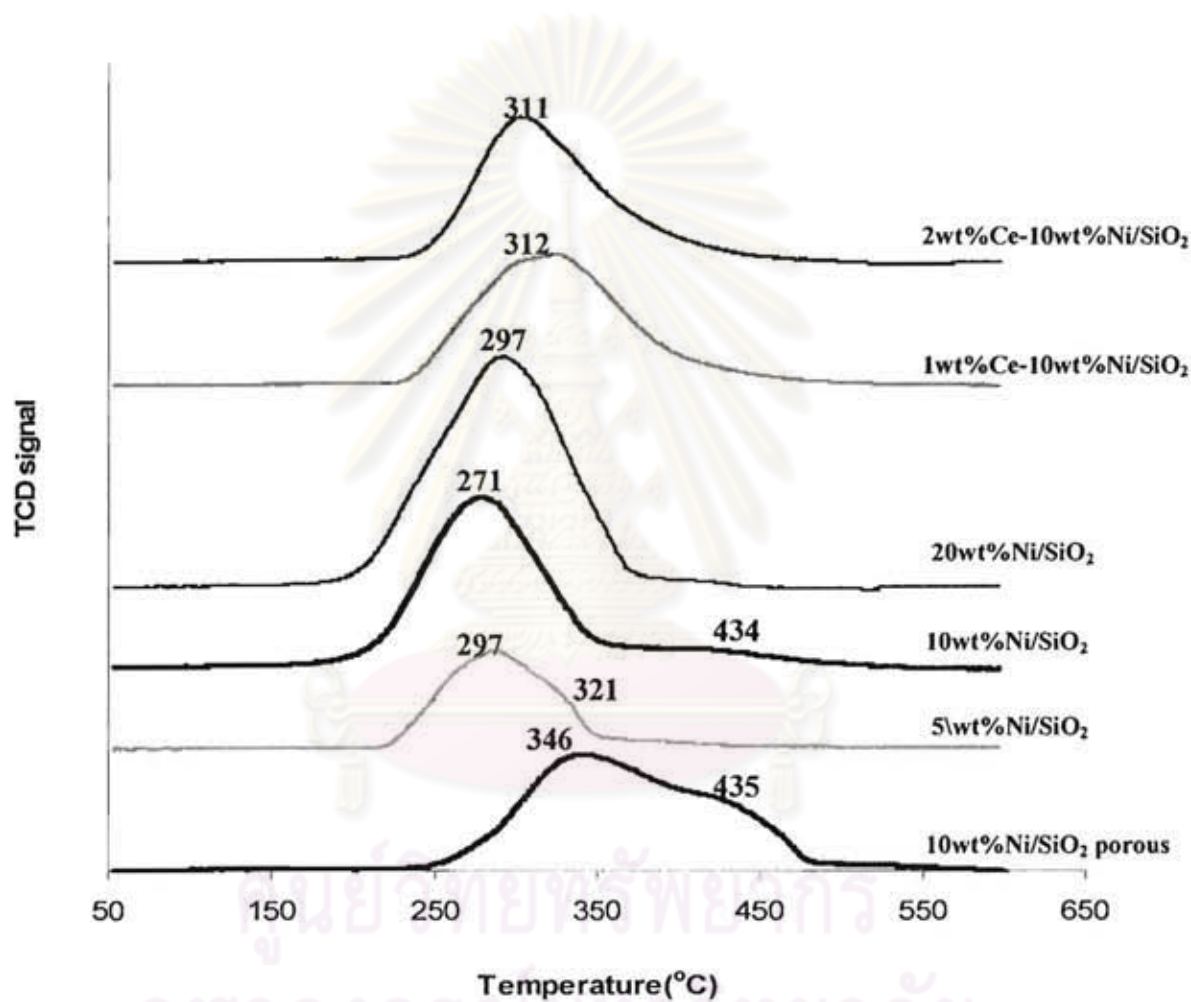
Figure 4.9 TPR profiles of Ni/SiO₂ fibers samples with varying Ni loading (5-20 wt%) and 10wt%Ni/SiO₂ with additional Ce loading (1 and 2 wt%).

Table 4.5 The H_2 TPR results

%Metal loading	Degree of Reduction (%)
5wt%Ni	87.38
10wt%Ni	95.80
20wt%Ni	67.0
1wt%Ce-10wt%Ni	89.88
2wt%Ce-10wt%Ni	82.90
10wt%Ni porous	98.80

4.2. Steam reforming reaction of glycerol

4.2.1 The effect of support: porous and fiber

Overall reaction $C_3H_8O_3 + 3H_2O \longleftrightarrow 3CO_2 + 7H_2$ ($\Delta H_o = +346.4$ kJ/mol)   (4.1)

Glycerol decomposition $C_3H_8O_3 \longleftrightarrow 3CO + 4H_2$ (4.2)

Water-Gas shift reaction $CO + H_2O \longleftrightarrow CO_2 + H_2$ (4.3)

Steam reforming of methane $CH_4 + H_2O \longleftrightarrow CO + 3H_2$ (4.4)
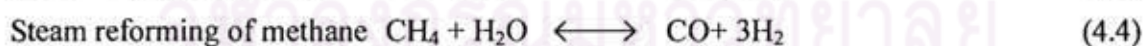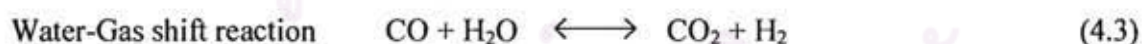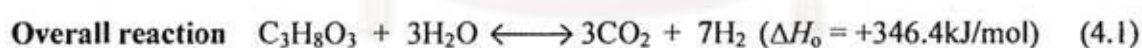
The influence of support in the process on the glycerol conversion over 10wt% Ni/SiO$_2$ catalyst was shown in figure 4.10(a). The result showed that when using the fiber as support for catalyst the glycerol conversion at 6h of reaction time was 92% that was 10% higher than the porous support. About the selectivity as can be observed in figure 4.10(b) and (c) the H_2 and CO_2 selectivity of porous support was higher than the fiber support while the fiber catalyst selective toward H_2 and CO that were 62 and 76%, respectively. This can be

attributed to the the fiber catalyst was selective to primary reaction in glycerol steam reforming as Eq.4.2 to produce H_2 and CO. In contrast to porous catalyst the H_2 and CO_2 selectivity were higher than fiber catalyst because of the water gas shift reaction which converts CO and water into CO_2 and H_2. The literature [22] proposed that the nickel metal activates organic molecules, by means of O-H, C-C and CH_2 bond breaking, and promotes the reaction between the organic fragments with OH groups from the water. The porous support with high surface area adsorbs the high content of water by the adsorption properties that can be gradually filled with liquid water by increasing the partial pressure confirmed by BET results. Meanwhile the fiber support which has no pore may adsorb the water molecules on the hydroxylated surface only as a multilayer by increasing the partial pressure without the condensation of water molecules thus the fiber support may not adsorb the water molecules enough to react with CO by water gas shift step thus the selectivities of H_2 and CO_2 were lower than the selectivities of H_2 and CO_2 of the porous support.

(a)

Figure 4.10 Effect of support on (a) glycerol conversion (b) H_2 selectivity (c) CO selectivity (d) CH_4 selectivity (e) CO_2 selectivity at a feed flow rate 0.01 mL/min, temperature 550°C catalyst loading 0.1 g, and W/G 9:1 at 6 h.

(b)

(c)

Figure 4.10 Effect of support on (a) glycerol conversion (b) H_2 selectivity (c) CO selectivity
(d) CH_4 selectivity (e) CO_2 selectivity at a feed flow rate 0.01 mL/min,
temperature 550°C catalyst loading 0.1 g, and W/G 9:1 at 6 h (continue).

(d)
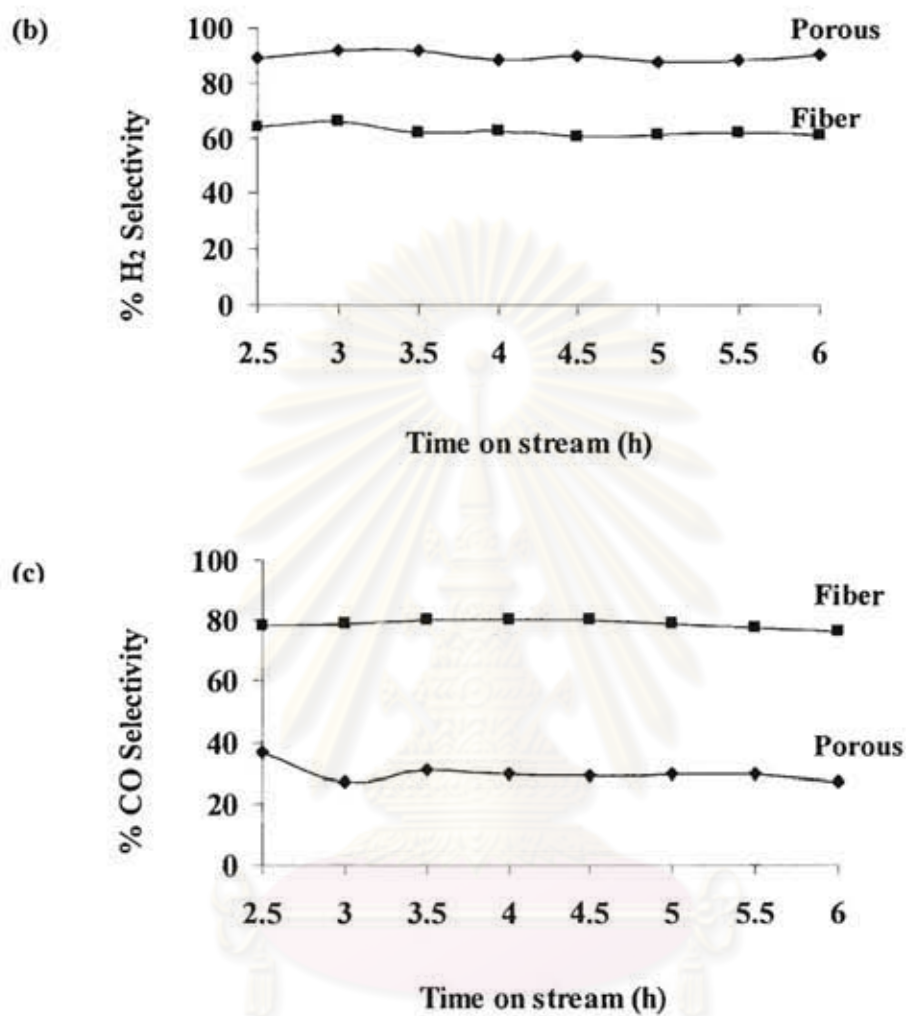
(e)

Figure 4.10 Effect of support on (a) glycerol conversion (b) H_2 selectivity (c) CO selectivity
(d) CH_4 selectivity (e) CO_2 selectivity at a feed flow rate 0.01 mL/min,
temperature 550°C catalyst loading 0.1 g, and W/G 9:1 at 6 h (continue).

4.2.2 The effect of reaction temperature

The influence of the temperature in the process on the glycerol conversion over 10wt% Ni/SiO_2 fiber catalyst was shown in figure 4.11. The conversion of glycerol increased with the increase in temperature and reached 88% as a maximum at 750°C since the steam reforming of glycerol is a highly endothermic reaction, the high temperature favors glycerol conversion.

Figure 4.12 showed the increasing temperature from 550 to 650°C and 650 to 750°C decreased H_2 selectivity significantly. The temperature of 550°C showed the highest H_2 selectivity of 62.75% followed by 34.92% at 650°C and 25.04% at 750°C. The fiber catalyst selected toward CO production that was always greater than 65% in all temperatures and CO_2 selectivity was found to be lower and decreased when the temperature was increased. This can be attributed to the fiber catalyst favors the primary reaction in glycerol steam reforming as Eq. 4.2 to produce H_2 and CO. As the reaction mechanism was described by Czernik [13] organic molecules adsorb on metal crystallite site, while water molecules support on the support surface. Hydrogen is produced via dehydrogenation of adsorbed organic molecules and reaction of adsorbed organic fragments with hydroxyl groups, which migrate from the support to the metal crystallite/support interfaces. The second reaction which is WGS reaction also results in the formation of carbon oxides. As a result, table 4.6 showed the lower of H_2 selectivity of 25.04% and CO_2 selectivity of 3.88% at 750°C. Other work [16] reported that increasing temperature increased H_2 selectivity. This can be attributed to the fact that at high temperature the water formed as a multilayer at the surface of silica fiber support was desorbed faster than low temperature thus the fiber catalyst has not enough water molecule to react with CO in water gas shift reaction leading to the higher CO in effluent gas. The more water content, the higher H_2 and CO_2 selectivity therefore the selectivity at low temperature was preferred by the fiber catalyst. In case of CH_4 selectivity, the increasing of that with increased reaction temperatures, reaching to 12.76% at 750°C. Obviously, the formation of methane in the glycerol reforming is not desirable because it reduces the selectivity towards H_2. On the other hand, the CH_4 selectivity decreased with increased reaction temperature due to the methane steam reforming at high temperature [16].

Additionally, the undesirable products as ethane and ethylene were also found to be increased when the reaction temperature increased. This can be attributed to the reaction catalyzed by fiber catalyst which has no pore occurred too fast thus the effluent with various products was possible.
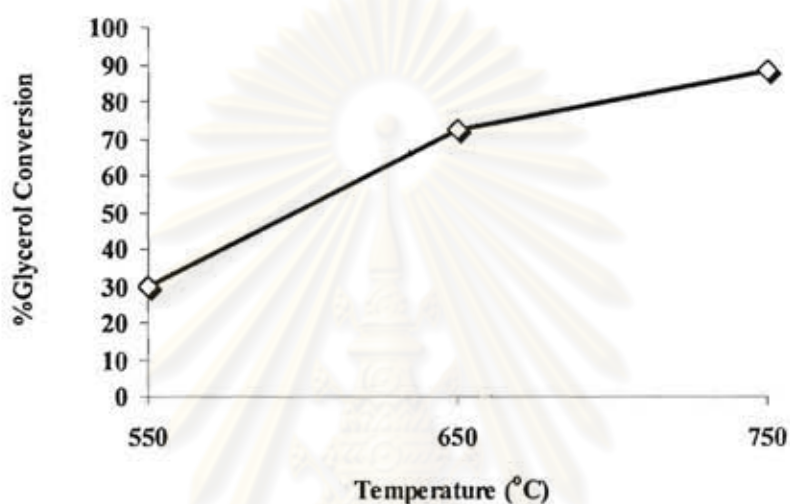
Figure 4.11 Effect of temperature on glycerol conversion at a feed flow rate 0.05 mL/min, catalyst loading 0.1 g, and W/G 6:1
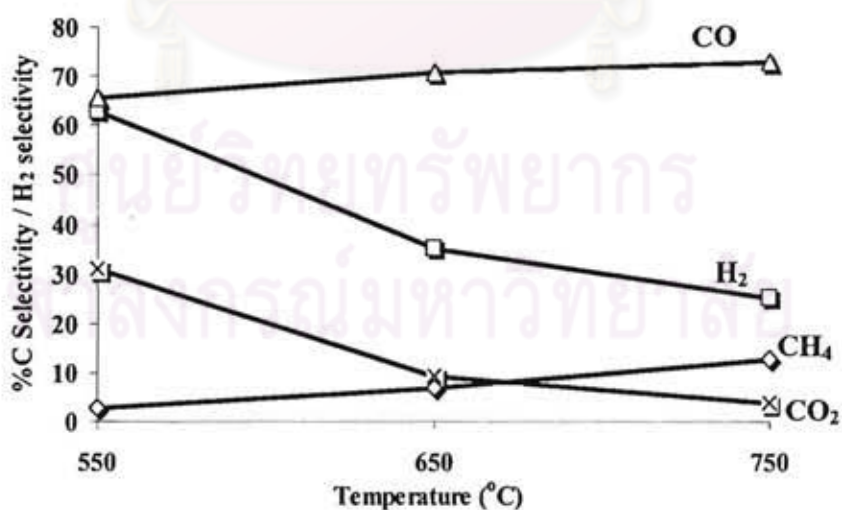
Figure 4.12 Effect of temperature on the selectivity of produced gas at a feed flow rate 0.05 mL/min, catalyst loading 0.1 g, and W/G 6:1
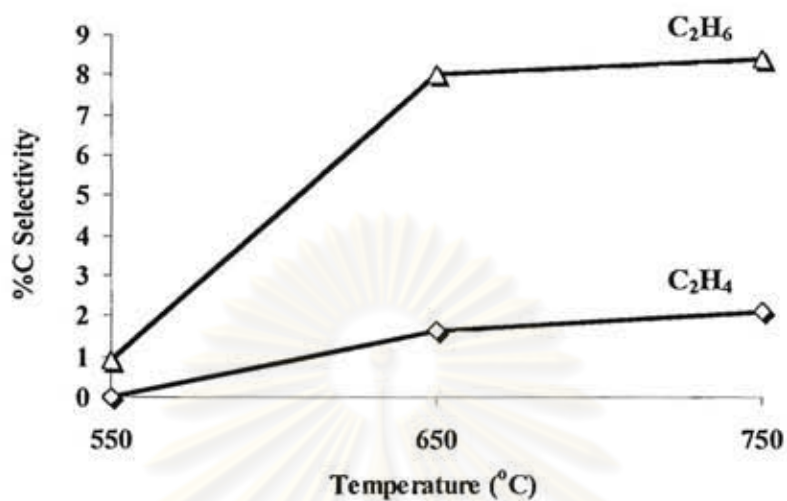
Figure 4.13 Effect of temperature on the selectivity of gas production at a feed flow rate 0.05 mL/min, catalyst loading 0.1 g, and W/G 6:1

Table 4.6 The effect of temperature on the glycerol conversion and gas product selectivity

Temperature (°C)	Conversion (%)	%Selectivity					
		H_2	CO	CO_2	CH_4	C_2H_6	C_2H_4
550	28.01	62.75	65.55	30.8	2.75	0.9	0
650	63.08	34.99	70.68	9.38	6.97	11.37	1.60
750	88.54	25.04	72.87	3.88	12.76	8.41	2.09

4.2.3 Feed flow rate Effect

Three different flow rates (0.01 0.03 and 0.05 mL/min) were used to investigate the effect of the feed flow rate (FFR) in terms of glycerol conversion and the H_2 selectivity for the 10wt%Ni/SiO_2 fiber catalyst. The glycerol conversion increased with a decrease in flow rate shown in figure 4.14. With the increase in feed flow rate from 0.01 to 0.03 mL/min, the conversion dropped from 70.65% to 52.19%. Further increase in feed flow rate to 0.05 mL/min, the conversion dropped to 28.01%.

Figure 4.15 showed the effect of the feed flow rate in H_2, CO, CO_2 and CH_4 selectivity. With the increase in feed flow rate from 0.01 to 0.03 mL/min, the H_2 did not change but CO_2 selectivity increased from 18.31 to 26.07. Further increase in 0.05 mL/min, the H_2 selectivity increased to 62.75% and CO_2 selectivity was increased to 30.8%. The CO selectivity was always greater than 65% in all fees flow rate. Other work [16] reported that increasing feed flow rate decreased H_2 selectivity. As mentioned earlier, this can be attributed to occurrence of the primary reaction in glycerol steam reforming as dictated by Eq. 2.5 and water gas shift reaction is a secondary reaction. As a result, the glycerol conversion decreased with increased in feed flow rate because the contact time which the substrate needs to contact with the catalyst to produce the selective product is shorter than the lower feed flow rate. Differently, H_2 selectivity and CO_2 selectivity increased with increasing feed flow rate probably due to high water content feeding in the reactor. This indicated that the selectivity of water gas shift reaction was increased.
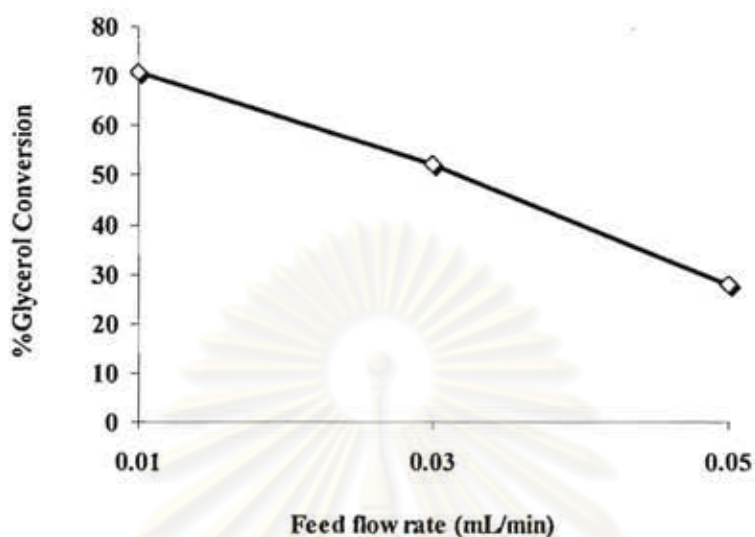
Figure 4.14 Effect of feed flow rate on glycerol conversion at a temperature 550°C, catalyst loading 0.1 g, and W/G 6:1 at 6 h.
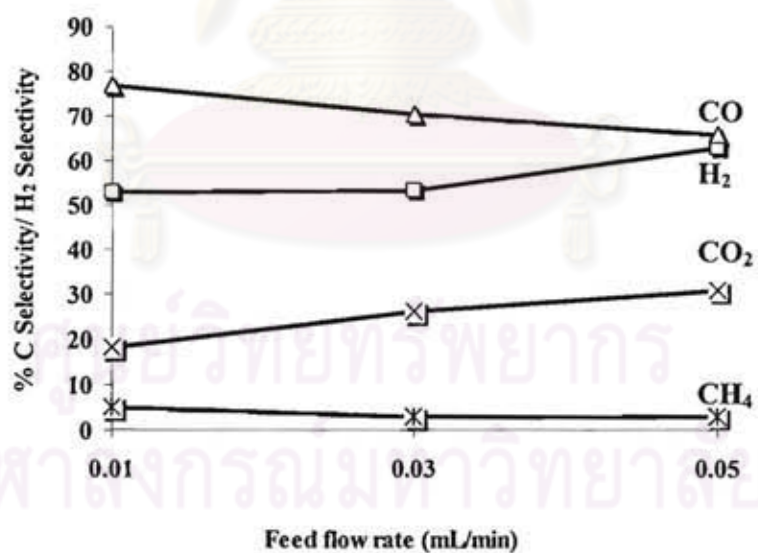
Figure 4.15 Effect of feed flow rate on the selectivity of produced gas at a temperature 550°C, catalyst loading 0.1 g, and W/G 6:1 at 6 h.

Table4.7 The effect of feed flow rate (FFR) on the glycerol conversion and gas product selectivity

FFR (mL/min)	%Conversion	%Selectivity					
		H_2	CO	CO_2	CH_4	C_2H_6	C_2H_4
0.01	70.65	52.93	76.62	18.31	5.07	0	0
0.03	52.19	53.32	70.47	26.07	2.75	0	0
0.05	28.01	62.75	65.55	30.8	2.75	0.9	0

4.2.4 Water/glycerol mole ratio effect

Figure 4.16 shows the effect of the water/glycerol mole ratio (W/G) in glycerol conversion catalyzed by the 10wt%Ni/SiO$_2$ fiber. With the increase in W/G, the glycerol conversion increased. With the increase in W/G from 3:1 to 6:1, the conversion increased from 47.99% to 70.65% and reached 92.45% at W/G 9:1. Figure 4.17 illustrated the effect of the WGMR in H_2, CO, CO_2 and CH_4 selectivity. The H_2 and CO_2 selectivity increased with increasing the W/G, whereas the CH_4 selectivity decreased with increasing W/G from 6:1 to 9:1. This can be attributed to the increasing of W/G leads to increase the H_2 and CO_2 selectivity due to the water gas shift reaction and leads to decrease the CH_4 selectivity due to the CH_4 reforming process. However, the reforming process consumed a considerable amount of energy with the increase in water mole ratio.
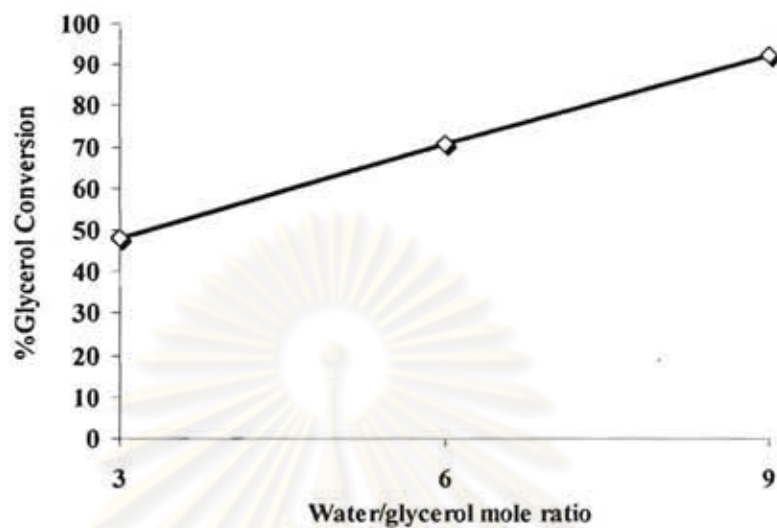
Figure 4.16 Effect of water/glycerol mole ratio on glycerol conversion at a temperature 550°C, catalyst loading 0.1 g, and feed flow rate 0.01 mL/min at 6 h.
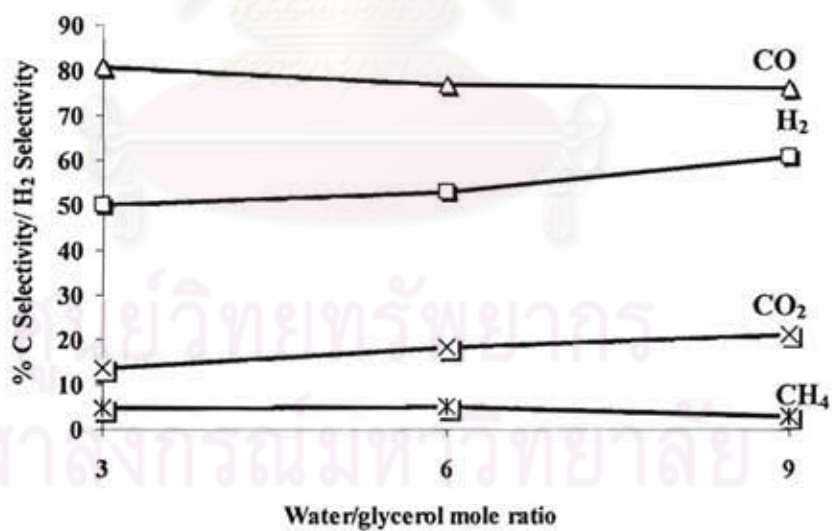
Figure 4.17 Effect of water/glycerol mole ratio on the selectivity of produced gas at a temperature 550°C, catalyst loading 0.1 g, and feed flow rate 0.01 mL/min at 6 h.

Table4.8 The effect of water/glycerol mole ratio (W/G) on the glycerol conversion and gas product selectivity

W/G	%Conversion	%Selectivity			
		H_2	CO	CO_2	CH_4
3:1	47.99	49.83	80.71	13.48	4.77
6:1	70.65	52.93	76.62	18.31	5.07
9:1	92.45	60.77	76.05	21.01	2.94

4.2.5 The effect of percentage of nickel loading

Catalyst with three different metal loadings (5, 10 and 20 wt%) were prepared by impregnation technique on the silica fiber as support to see the effect of the metal percentage on glycerol conversion as can be seen in figure 4.18 and selectivity of H_2 and other gaseous products in figure 4.19. The increase in metal loading from 5 to 10wt% increased glycerol conversion from 74.69 to 92.45%. Further increase in 20wt%, the glycerol conversion dropped to 60% due to the nickel particle of 20wt%Ni catalyst was larger than the 10wt%Ni catalyst affecting the decreasing of their surface area of active nickel. This indicated that the silica fiber support which has the average diameter size of 1.28 μm can be loaded the nickel content up to 10 percentages by weight because of the lower surface area of fiber to support the nickel particles as described above in the EDS result. In case of gases selectivity, the H_2 and CO_2 selectivity increased and CO and CH_4 selectivity decreased with increasing the metal loading.
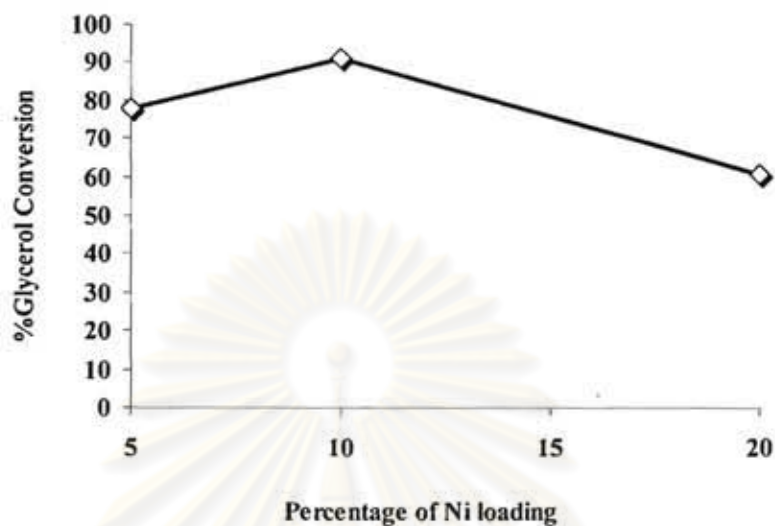
Figure 4.18 Effect of nickel loading on glycerol conversion at a temperature 550°C, W/G 9:1, catalyst loading 0.1 g, and feed flow rate 0.01 mL/min at 6h.
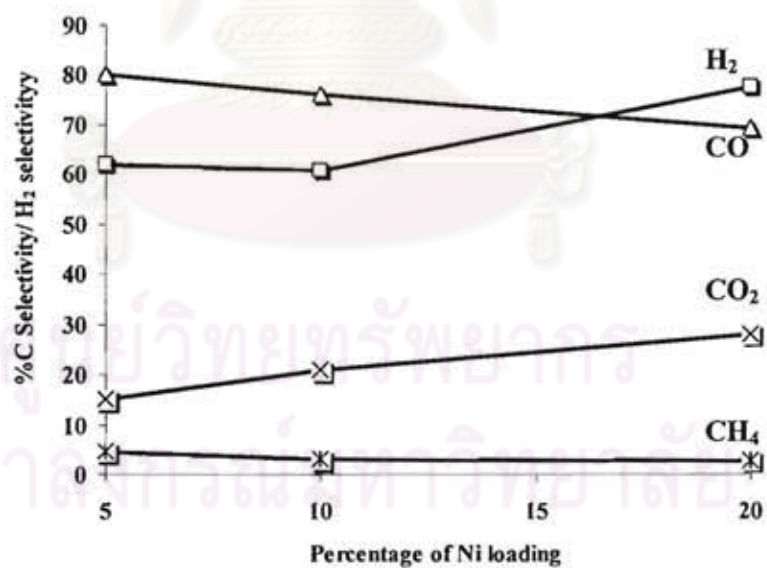
Figure 4.19 Effect of nickel loading on the selectivity of produced gas at temperature 550°C, W/G 9:1, catalyst loading 0.1 g, and feed flow rate 0.01 mL/min at 6 h.

Table 4.9 The effect of nickel loading on the glycerol conversion and gas product selectivity

%Ni loading	%Conversion	%Selectivity			
		H_2	CO	CO_2	CH_4
5	74.69	61.95	80.15	15.18	4.67
10	92.45	60.77	76.05	21.01	2.94
20	60.72	77.82	69.26	27.96	2.78

4.2.6 The effect of cerium addition

Figure 4.20 illustrated the effect of cerium on the glycerol conversion. It was observed that the conversion of glycerol decreased with increasing the cerium. With 1wt%Ce the glycerol conversion dropped from 92.45 to 73.61% and further dropped to 68.87% at 2wt%Ce. This can be contributed to the degree of reduction was decreased as described in the TPR results. Nevertheless, the CeO_2 can promote the performance of nickel catalyst in term of the increasing of CO_2 selectivity because of its natural redox properties which can be reduced in oxygen deficient conditions while oxidized in oxygen sufficient conditions. Figure 4.21 revealed the gases selectivity with the addition of Ce of 1wt% and 2wt% leading to the no significant increasing of H_2 selectivity. Differently, the CO_2 selectivity increased continuously with increasing the Ce loading. The improved catalytic performance of the 10wt%Ni/SiO$_2$ catalyst could be attributed to a strong interaction between Ni and Ce, as described in the TPR results. Meanwhile the CO selectivity decreased with increasing the percentage of cerium. This could be attributed to the efficient water gas shift reaction promoted by the high OH group surface mobility of CeO_2 which is related to the ceria-mediated redox process. Specially, CO adsorbed on Ni particles reduced ceria surface to generate CO_2, and water reoxidized the ceria surface to CeO_2, releasing H_2.
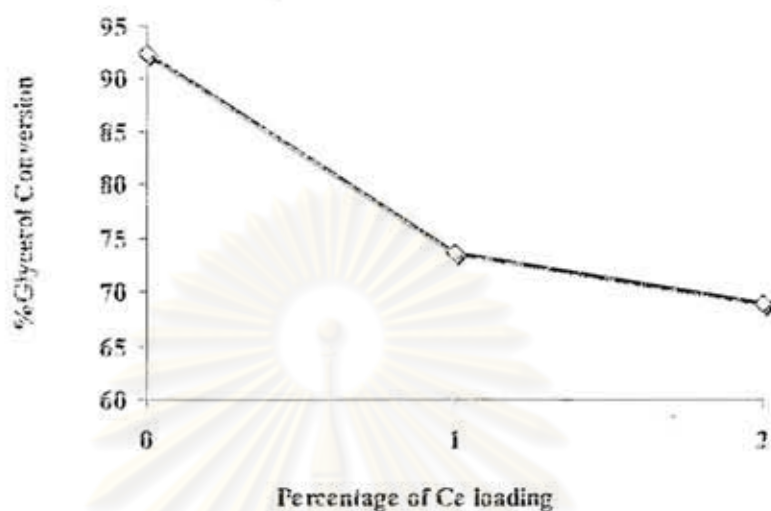
Figure 4.20 Effect of Ce loading of 10wt%Ni/SiO$_2$ on glycerol conversion at a temperature 550°C, W/G 9:1, catalyst loading 0.1 g, and feed flow rate 0.01 mL/min at 6 h.
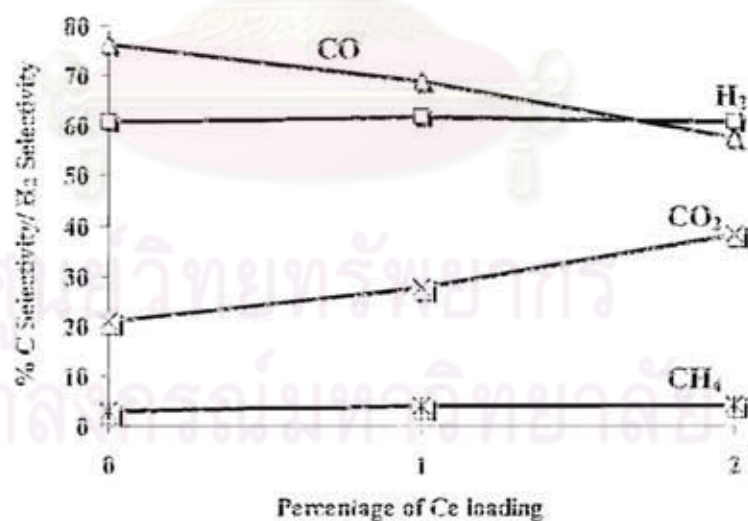
Figure 4.21 Effect of Ce loading of 10wt%Ni/SiO$_2$ on the selectivity of produced gas at a temperature 550°C, W/G 9:1, catalyst loading 0.1 g, and feed flow rate 0.01 mL/min at 6 h.

Table 4.10 The effect of Ce on the glycerol conversion and gas product selectivity

%Ce	%Conversion	%Selectivity			
		H_2	CO	CO_2	CH_4
0	92.45	60.77	76.05	21.01	2.94
1	73.61	61.73	68.7	27.48	3.83
2	68.87	60.65	57.61	38.27	4.12

In this research the 10wt%Ni/SiO$_2$ was found to be the best performing catalyst under the experimental at 550°C, W/G 9:1 and feed flow rate 0.01 mL/min investigated.

4.2.7 The coke formation

The SEM micrographs showing the morphological appearance of the used catalyst after operation in a fixed-bed reactor are shown in figure 4.22 (b). The presence of filamentous carbon, a few nanometers in diameter and several micrometers long, is clearly evidenced. Deposited carbon also appears as uniform coating on Ni particles that could reduce the lifetime of the catalysts. The mechanism proposed in the literature [18] at lower temperature, filamentous carbon was formed by formation of carbon atoms from methane on the surface of Ni particles and followed by the diffusion of carbon atoms through the Ni particles. The filamentous carbon diameter is governed by the dimensions of the metal particle while the length depends largely on the duration of reaction.

The results of TEM observation of carbon filamentous formed on Ni/SiO$_2$ catalyst was shown in figure 4.23. It is the carbon filament that Ni metal particles anchored on the tip and encapsulated inside the carbon filament. It has been suggest that the weak interaction would result in the formation of carbon filament filled with the metal particles [30].

The morphology of the catalyst after coke removal was shown in figure 4.22 (c). It was the carbon deposited that can be completely removed by the oxidation with air at 700°C for 1 h referred to the TGA result in figure 4.24 which was examined to analyze the oxidation temperature of the carbon. In case of the porous catalyst there are two temperature ranges at

280 and 575°C observed as the oxidation temperature of the carbon deposited. It means that there are two types of coke deposited. The first was attributed to the carbon as the soft coke that can be easily removed by oxidation at a relative lower temperature and the second, hard coke or the coke that was much more refractory and adsorbed strongly on the catalyst surface [31], can be removed at high temperature. In case of the fiber catalyst there are two temperature ranges of the carbon decomposition as the porous but the both of oxidation temperature shifted to lower temperature indicating that the carbon filament depositing on the fiber catalyst surface could be easily removed at temperature lower than the carbon deposited on the porous catalyst.

The XRD pattern of used catalyst was shown in figure 4.25. The characteristic peaks corresponding to (111), (200), (220), (311) and (222) crystal planes of NiO were the same as fresh catalyst but the peaks were found to be sharper indicating that NiO of used catalyst has the larger particle size from 11.37 to 20.31 nm due to the gradual aggregation of Ni crystalline departing into particles by dissociation of carbon deposited [25].
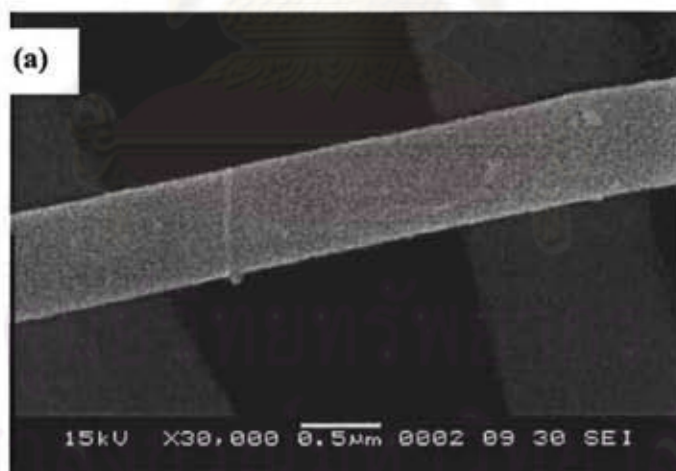
Figure 4.22 SEM images of (a) 10wt%Ni/SiO$_2$ fresh catalyst (b) used catalyst after 6 h
(c) used catalyst with coke removal.
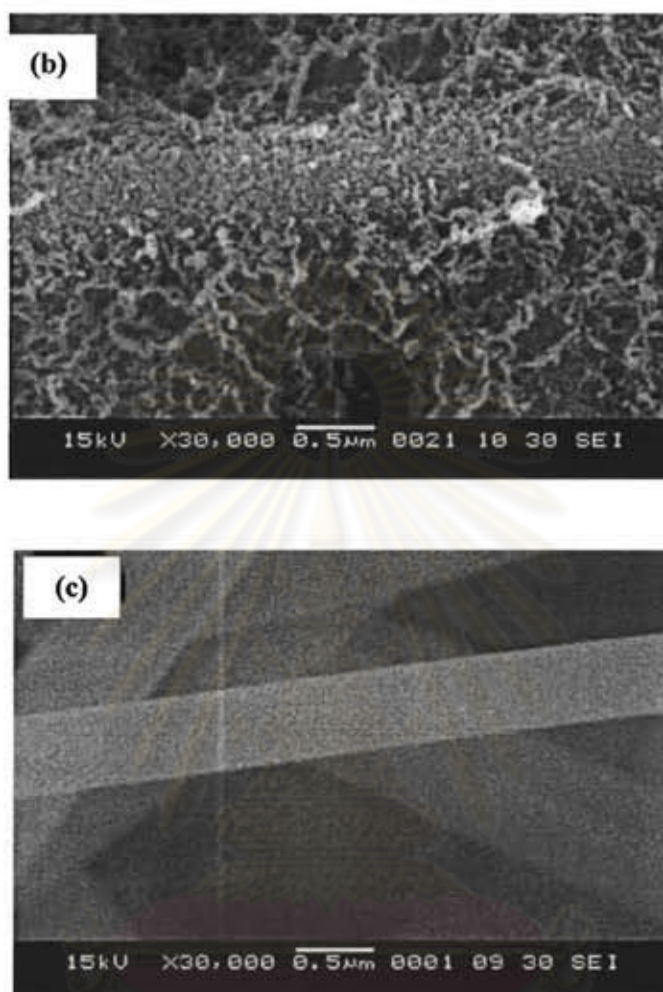
Figure 4.22 SEM images of (a) 10wt%Ni/SiO₂ fresh catalyst (b) used catalyst after 6 h
(c) used catalyst with coke removal.(continue)
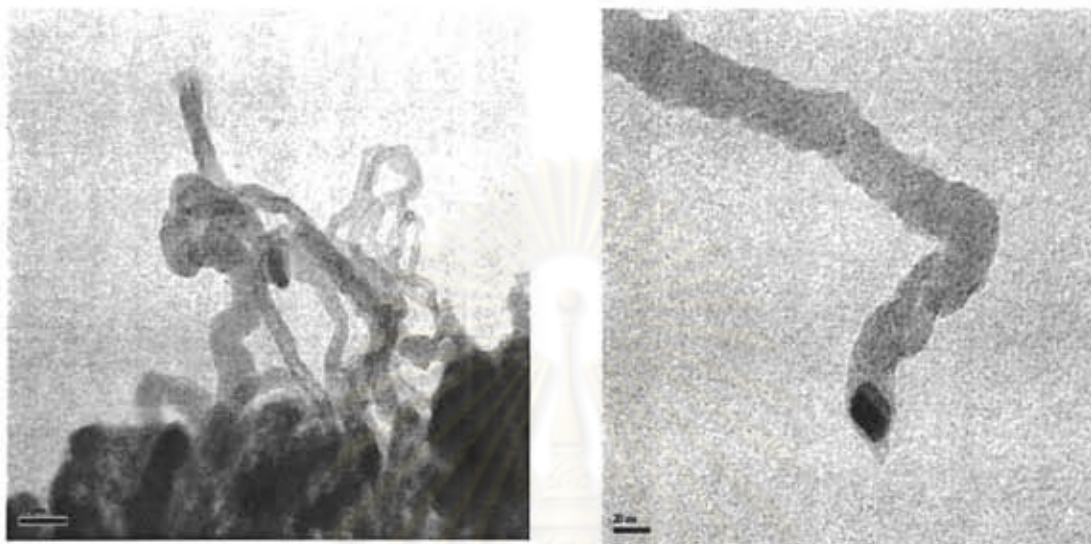
Figure 4.23 TEM images of carbon nanofiber
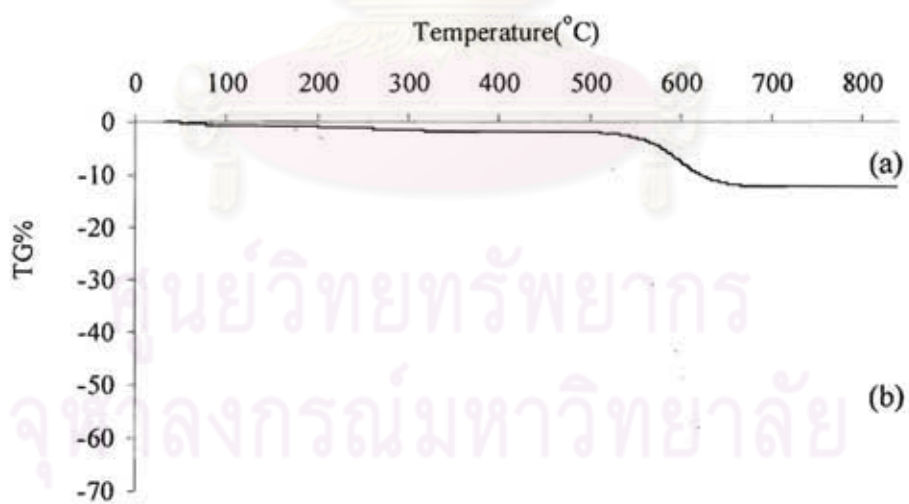
Figure 4.24 TGA profile of used catalyst of 10wt%Ni/SiO$_2$ (a) porous and (b) fiber
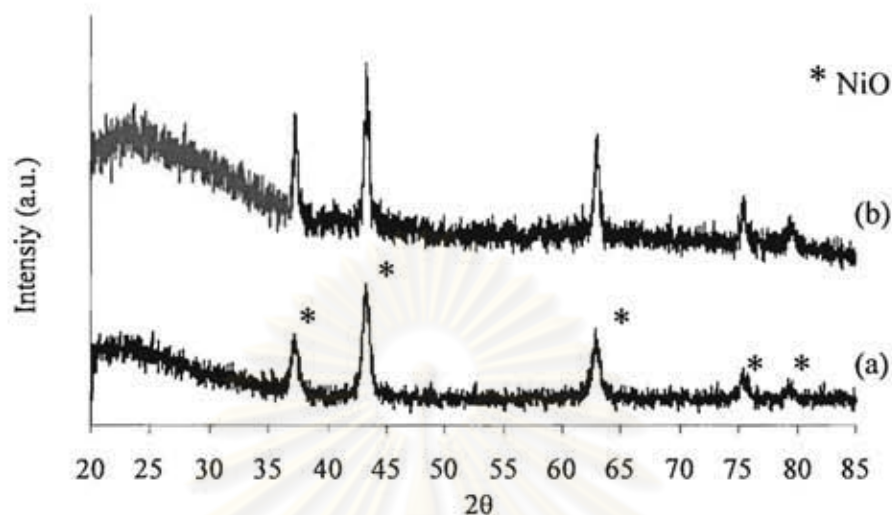
Figure 4.25 XRD patterns of 10wt%Ni/SiO$_2$ (a) fresh and (b) used catalyst after coke removal

The TPR profile of 10wt%Ni/SiO$_2$ fiber catalyst before and after reforming reaction was illustrated in figure 4.26. The TPR profile of used catalyst after reformig reaction for 6 h was found the two reduction peaks at 363 and 494°C compared with the 10wt%Ni/SiO$_2$ before reaction, the reduction peaks shifted to high temperature due to the phase NiO of used catalyst has stronger interaction between NiO and oxide support. Additionally, the reduction degree was decreased from 98.51 to 72.95% after reaction. This can be attributed to the large crystallite size of NiO after reaction confirmed by XRD result in figure 4.25.
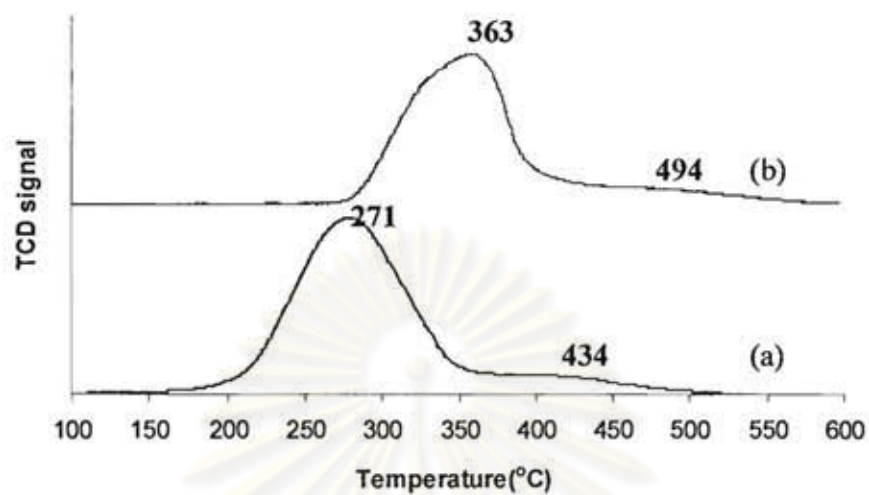
Figure 4.26 TPR profiles of 10wt%Ni/SiO$_2$ fibers sample (a) fresh catalyst after calcination (b) used catalyst for 6h after coke removal

CHAPTER V

CONCLUSION AND RECOMMENDATION

5.1 Conclusion

The nickel/silica fiber catalysts have been produced by combining sol-gel synthesis and electrospinning technique using TEOS as a source of silica by the molar ratio of TEOS: ethanol: H_2O: HCl of 1:2:2:0.01 and then the silica fiber was impregnated by nickel acetate solution. The electrospun fiber showed the average diameter 0.93 μm. XRD results showed the amorphous structure of pure silica fibers and there is crystalline structure for the fiber added nickel under calcination process. The chemical composition was confirmed by EDS results. The TPR profiles of nickel/silica fiber catalysts revealed the reduction peak of NiO at 271°C which shifted to the lower temperature compared to that of nickel/silica porous catalysts (346°C) indicating that the fiber catalyst was easily reduced than the porous catalyst. The catalyst activity tests on the hydrogen production from steam reforming of glycerol were studied. The results showed that the fibers are significantly active and selective for H_2 and CO production from steam reforming reactions of glycerol whereas the porous catalyst was selective for H_2 and CO_2. This can be attributed to the fiber catalyst was less selective toward the WGS reaction due to it can adsorb the water molecules less than the porous catalyst. Furthermore, when increasingly added CeO_2 the selectivity of CO_2 was increased significantly due to the CeO_2 helps the performance of Ni as the source of oxygen based on the ceria redox process. The characterization of used catalyst found the carbon nanofiber around the catalyst surface which can be completely removed by oxidation with air at 700°C for 1 h and the Ni crystallite size of the used catalyst after coke removal was larger than fresh catalyst due to the aggregation.

5.2 Recommendation

For the future research work, the development of the electrospinning process to produce the fiber in small diameter by decreasing the needle diameter should be greatly used as the support due to the higher surface area per volume catalyst. The improvement of the water gas shift activity of the catalyst by Fe and Zr addition and the modification of nickel based catalyst by Sn addition which could lower the carbon deposition should be investigated.

REFERENCES

[1] Yazhon, C., Hengyong, X., Yuzhong, W., Xianglan, J. and Guoxing, X. Hydrogen production from liquid hydrocarbon fuels for PEMFC application. Fuel Processing Technology. 87: (2006) 971-978.

[2] Koroneos, C., Dompros, A., Roumbas, G. And Moussiopoulos, N. Life cycle assessment of hydrogen fuel production processes. International Journal of Hydrogen Energy. 29: (2004) 1443-1450.

[3] Formhals, A. Process and apparatus for preparing artificial threads. US Patent 1975504
(1934)

[4] Reneker, DH. And Chun, I. Nanometre diameter fibes of polymer produced by electrospinning. Nanotechnology 7(1996): 216-23.

[5] Chronakis, S. Novel nanocomposites and nanoceramics based on polymer nanofibers using electrospinning process-review. Journal of Materials Processing Technology. 167: (2005) 283-293.

[6] Lee, S., Kim, Y., Choi, S., Park, T., Joo, Y., and Lee, S. Preparation of SiO_2/TiO_2 composite fibers by sol-gel reaction and electrospinning. Materials letters. 61: (2007) 889-893.

[7] Choi S. Titania-Doped silica fibers prepared by electrospinning and sol-gel process. Journal of Sol-gel Science and Technology. 30: (2004) 215-221.

[8] Joo, Y. and Panels, J. Incorporation of vanadium oxide in silica nanofiber mat via electrospinning and sol-gel synthesis. Journal of Nanomaterials. (2006) 1-10.

[9] Sumio, S. Sol-gel science and technology: processing characterization and applications. Moscow: Kluwer Academic Plublishers,.

[10] Fong, H. Beaded nanofibers formed during electrospinning. Polymer. 40: (1999) 4585-4592.

[11] Brown, P.J. and Stevens, K. Nanofibers and nanotechnology in textiles. New York: Woodhead plublishing limited, 2007.

[12] Frenot, A. and Chronakis, S. Polymer nanofibers assembled by electrospinning.

Current Opinion in Colloid and Interface Science 8: (2003) 64-75..

[13] Czernik, S. Hydrogen by catalytic steam reforming of liquid byproducts from biomass thermoconversion processes. Industrial and Engineering Chemistry Research 41: (2002) 4209-4215.

[14] Jens, S. Four challenges for nickel steam-reforming catalysts. Catalysis Today. 111: (2006) 103-110.

[15] Zhang, B., Tang, X., Li, Y., Xu, Y. and Shen, W. Hydrogen production from steam reforming of ethanol and glycerol over ceria-supported metal catalysts. International Journal of Hydrogen Energy. 32: (2007) 2367-2373.

[16] Adhikari, S., Fernando, S., To, S.D., Bricka, R., Steele, P. and Haryanto, A. Conversion of glycerol to hydrogen via a steam reforming process over nickel catalyst. Energy&Fuels. 22: (2008) 1220-1226.

[17] Deitzel, J.M., Kleinmeyer, D., Harris, D. and Beck Tan N.C. The effect of processing variables on the morphology of electrospun nanofibers and textiles. Polymer. 42: (2001) 261-272.

[18] Takenaka, S., Kobayashi, S., Ogihara, H. and Otsuka, K. Ni/SiO$_2$ catalyst effective for methane decomposition into hydrogen and carbon nanofiber. Journal of Catalysis. 217: (2003) 79-87.

[19] Peng, K., Zhou, L., Hu, A., Tang, Y. and Li, D. Synthesis and magnetic properties of Ni-SiO$_2$ nanocomposites. Material Chemistry and Physics. 111: (2008) 34-37.

[20] Adhikari, S., Fernando, S. and Haryanto, A. Production of hydrogen by steam reforming of glycerine over alumina-supported metal catalysts. Catalysis today. 129: (2007) 355-364.

[21] Li, X., Li, Z. and Xi, H. Effects of pore sizes of porous silica gels on desorption activation energy of water vapour. Applied Thermal Engineer. 27: (2007) 869-876.

[22] Dong, W. and Roh, H., Methane reforming over Ni/Ce-ZrO$_2$ catalysts: effect of nickel content. Applied catalysis A: General. 226: (2002) 63-72.

[23] Biswas, P. and Kunzru, D. Steam reforming of ethanol for production of hydrogen over Ni/CeO$_2$-ZrO$_2$ catalyst: effect of support and metal loading. International Journal of Hydrogen Energy. 32: (2007) 969-980.

[24] Sanchez, M.C and Navarro, R.M. Ethanol steam reforming over Ni/MxOy-Al$_2$O$_3$ (M=Ce, La, Zr and Mg) catalysts: Influence of support on the hydrogen production. International Journal of Hydrogen Energy. 32 (2007) 1462-1471.

[25] Li, Y., Zhang, B., Xie, X., Liu, J., Xu, Y. and Shen, W. Novel Ni catalysts for methane decomposition to hydrogen and carbon nanofibers. Journal of Catalysis. 238: (2006) 412-424.

[26] GaO, L., Sun, G. and Kawi, S. A study on methanol steam reforming to CO$_2$ and H$_2$ over the La$_2$CuO$_4$ nanofiber catalyst. Journal of Solid State Chemistry. 181: (2008) 7-13.

[27] Kim, H., Choi, Y., Kanuka, N. and Kinoshita, H. Preparation of Pt-loaded TiO$_2$ nanofibers by electrospinning and their application for WGS reaction. Applied Catalysis A: General. 352: (2009) 265-270.

[28] Pereira, E., Homs, N., Marti, S., Fierro, J.L.G. and Piscina, P. Oxidative stem-reforming of ethanol over Co/SiO$_2$, Co-Rh/SiO$_2$ and Co-Ru/SiO$_2$ catalysts: Catalytic behavior and deactivation/regeneration processes. Journal of Catalysis. 257: (2008) 206-214.

[29] Deraz, N.M., Selim, M.M. and Ramadan, M. Processing and properties of nanocrystalline Ni and NiO catalysts. Materials Chemistry and Physics. 113: (2009) 269-275.

[30] Takehira, K., Ohi, T., Shishido, T., Kawabata, T. and Takaki, K. Catalytic growth of carbon fibers from methane and ethylene on carbon-supported Ni catalysts. Applied Catalysis A: General. 283: (2005) 137-145.

[31] Edward Furimsky. Catalyst for upgrading heavy petroleum feeds. United Kingdom: Elsevier, 2007.

APPENDICES

Appendix A

Calculation for Preparation of 10wt%Ni/SiO₂ fiber catalyst

10wt%Ni/SiO$_2$ fiber catalyst was prepared by electrospinning-impregnation method

1st step: electrospinning (sol-gel)

TEOS 1 mol = silica 1 mol

Silica(MW = 60.09 g/mol) 1mol = 60.09 g

TEOS(MW = 208.33 g/mol) 1mol = 208.33 g

Basis 7.5 g of silica

Therefore   weight of TEOS = (208.33 x 7.5)/60.09 = 26.00 g = 26.00/208.33 = 0.1248 mol

For Sol-gel   The mol ratio of TEOS:EtOH:H$_2$O:HCl = 1:2:2:0.01

From above TEOS = 0.1248 mol

Therefore TEOS:EtOH:H$_2$O:HCl = 0.1248: 0.2494: 0.2494: 1.2x10^{-3}

EtOH (MW = 46.07 and density = 0.789 g/cm^3)

      0.2494 mol = (0.2494 x 46.07)/0.789 = 14.56 mL

H$_2$O (MW = 18 and density = 1 g/cm^3)

      0.2494mol = (0.2494 x 18)/1 = 4.49 mL

HCl (MW= 36.46 and density = 1.18 g/cm^3)

      1.2x10^{-3} mol = (1.2x10^{-3} x 36.46)/1.18 = 0.04 mL

TEOS (purity = 98% and density = 0.93 g/cm^3)

From   mol = (10 x Density x purity x volume)/(1000 x MW)

Therefore TEOS 0.1248 mol = (10 x 0.93 x 98 x Volume)/(1000 x 208.33)

         Volume = 27.93 mL

2nd step: impregnation

Using the nickel acetate (Ni(CH$_3$COO)$_2$.4H$_2$O) as a precursor

For 10wt%Ni/SiO$_2$

Basis 0.2167 g of silica fiber

Therefore   weight of Ni = (10 x 0.2167)/100 = 0.02167 g

Ni 1 mol = Ni(CH$_3$COO)$_2$.4H$_2$O 1 mol

Ni(CH$_3$COO)$_2$.4H$_2$O (MW = 248.86 g/mol) and Ni (MW = 58.69 g/mol)

Therefore   weight of Ni(CH$_3$COO)$_2$.4H$_2$O = (248.86 x 0.02167)/58.69 = 0.092 g

Calculation for the surface area of SiO$_2$ fiber

Silica fiber produced by the applied voltage of 15 kV and the TCD of 15 cm

Average diameter (from SEM image) = 1.27 μm, radius = 0.635 μm

Density of SiO$_2$ = 2.1 g/cm^3

Surface area = m^2/g = m^2/density x Volume = (2πr x length)/(density x πr^2 x length)

$\qquad$ = 2/density x r

$\qquad$ = 2/(2.1g/cm^3 x 0.635 μm) = 1.49 m^2/g

Calculation of reduction degree

10wt%Ni/SiO$_2$

Basis 0.2067 g of silica fiber prepared by impregnating Ni(CH$_3$COO)$_2$.4H$_2$O

(MW = 248.86 g/mol) = 0.092 g

NiO 1 mol = Ni(CH$_3$COO)$_2$.4H$_2$O 1 mol

NiO (MW = 74.69 g/mol)

Therefore weight of NiO = (74.69 x 0.092)/248.86 = 0.0276 g in 0.2067 g of catalyst

The weight of catalyst for TPR analyzing = 0.0914 g

If catalyst 0.0914 g   mol of NiO = ((0.0914 x 0.0276)/0.2067)/74.69 = 1.63 x 10^{-4} mol

From TPR result

Using 10%H$_2$ in Ar as carrier gas and flow rate 50 mL/min

Calculated the mol of H$_2$ input = (10 x 50)/(100 x 22400) = 2.23 x 10^{-4} mol

The mol $H_2 = 2.23 \times 10^{-4}$, the area = 0.6233

If the Area below curve = 0.4496

Therefore H_2 consumption = $(2.23 \times 10^{-4} \times 0.4496)/0.6233 = 1.61 \times 10^{-4}$ mol

The percentage of reduction of $10wt\%Ni/SiO_2$

    = 100 x mol of H_2 consumption/mol of H_2 loading

    = 100 x $(1.61 \times 10^{-4}/1.63 \times 10^{-4})$ = 98.51

Calculation of glycerol conversion and gas product selectivity

Reaction conditions: Water/glycerol mole ratio 9:1 and feed flow rate 0.01 mL/min

At 6 h flow rate output = 18.12 mL/min

As   Area Standard $1\%H_2$ = 99562.6   Area H_2 = 1415209.8

                $1\%CO$ = 5156.3   CO = 39307.1

                $1\%CH_4$ = 20745 CH_4 = 6113.6

                $1\%CO_2$ = 9488.1 CO_2 = 19983.1

Therefore

Mole of H_2 gas   = Area H_2/Area std H_2 = 1415209.8/99562.6 = 14.21 %

                    = $((14.21/100) \times 18.12)/22400 = 1.15 \times 10^{-4}$ mol/min

Mole of CO gas   = Area CO/Area std CO = 39307.1/5156.3= 7.62 %

                    = $((7.62/100) \times 18.12)/22400 = 6.17 \times 10^{-5}$ mol/min

Mole of CH_4 gas   = Area CH_4/Area std CH_4 = 6113.6/20745= 0.29 %

                    = $((0.29/100) \times 18.12)/22400 = 2.38 \times 10^{-6}$ mol/min

Mole of CO_2 gas   = Area CO_2/Area std CO_2 = 19983.1/9488.1 = 2.1 %

                    = $((2.1/100) \times 18.12)/22400 = 1.7 \times 10^{-5}$ mol/min

Mole of C atom total = $(CO + CH_4 + CO_2)$

                    = $6.17 \times 10^{-5} + 2.38 \times 10^{-6} + 1.7 \times 10^{-5} = 8.11 \times 10^{-5}$ mol/min

Therefore

H_2 selectivity (%) $\quad = ((1.15 \times 10^{-4}/8.11 \times 10^{-5})/(7/3)) \times 100 = 60.72\%$

CO selectivity (%) $\quad = (6.17 \times 10^{-5} \times 8.11 \times 10^{-5}) \times 100 = 76.05\%$

CH_4 selectivity (%) $\quad = (2.38 \times 10^{-6} \times 8.11 \times 10^{-5}) \times 100 = 2.93\%$

CO_2 selectivity (%) $\quad = (1.7 \times 10^{-5} \times 8.11 \times 10^{-5}) \times 100 = 21.01\%$

GHSV = 12,000 ml/g_{cat} hr = 200 ml/g_{cat} min

Catalyst = 0.1 g

V = 22.4 lit (STP) = 22400 ml (STP)

Water/glycerol mol ratio = 9:1

	mole fraction	Vapor ml/min	mol/min
Glycerol	0.03	0.6	0.000029236
H_2O	0.27	5.4	0.000263148
N_2	0.7	14	0.000682234
Total	1	20	0.000974621

Glycerol input = $2.92 \times 10^{-5} \times 3 = 8.77 \times 10^{-5}$ mol/min

Glycerol conversion (%)

$\quad$ = (mole C atom total in gas product/ mole glycerol input) x 100

$\quad$ = $(8.11 \times 10^{-5}/ 8.77 \times 10^{-5}) \times 100 = 92.45\%$

Appendix B
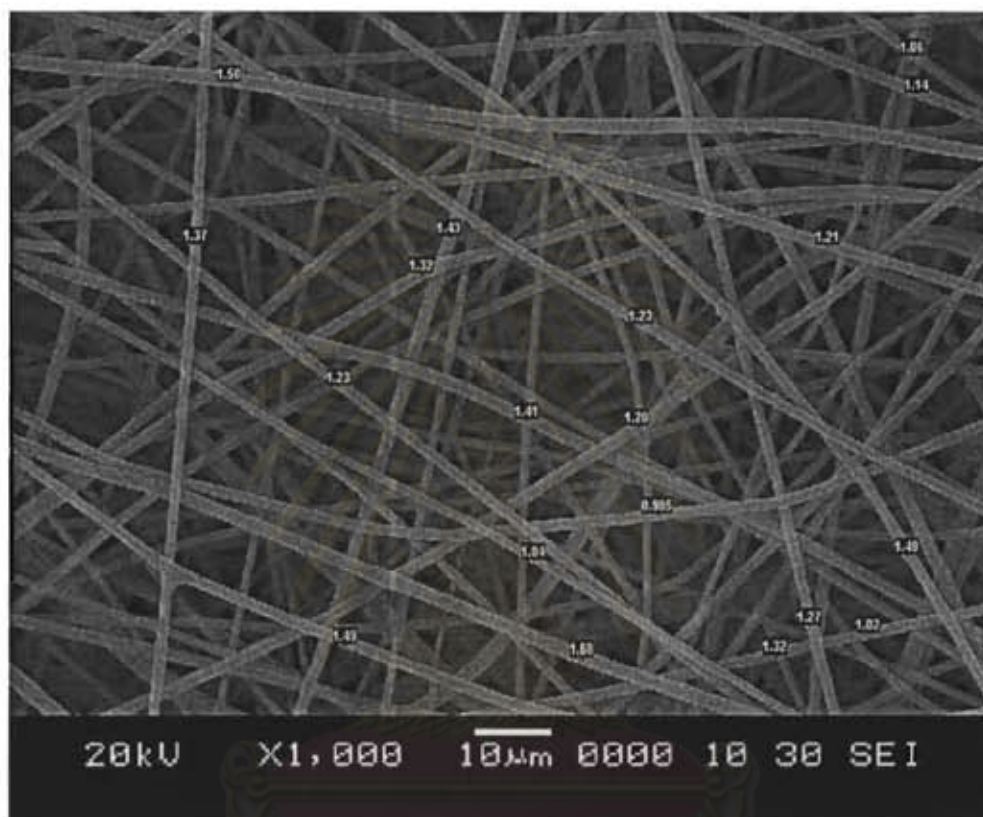
Figure B-1 Determination of fiber diameter by SemAfore program

Table B-1 Determination of glycerol conversion and gas product selectivity

Data from the use of catalyst: $10wt\%Ni/SiO_2$, $T_{reaction}$ = 750°C W/G= 6:1 feed flow rate = 0.05 mL/min

Standard gas composition

$1\%H_2$ $1\%CO$ $1\%CO_2$ $1\%CH_4$ $1\%C_2H_6$ $1\%C_2H_4$ Balance in N_2

Area	std	2.5	3	3.5	4	4.5	5	5.5	6
H_2	97253.5	2805210	2878695	2841219	2634556	2786524	2687128	2682673	2679540
CO	5000.5	174057	177937.3	171594.2	168461.6	164066	174070	180717.7	171819.8
CH_4	19599.1	102596.3	109734.6	107048	106215.7	107941.7	113841.9	122560.3	117881.2
CO_2	9862	22779.8	23017.3	21984	20020.8	21923.1	21425.4	20825.9	18039.9
C_2H_4	17048.2	15647.7	19266.6	22471	23808.5	28605.4	30109.1	34084.5	35456
C_2H_6	18755.3	7204.3	7291.6	8353	8356.3	9294.4	9255.3	9745.2	9701.2

Hour		2.5	3	3.5	4	4.5	5	5.5	6
	H_2	7.84	7.73	8.24	7.74	7.90	7.86	7.74	7.69
	CO	5.10	4.88	4.73	4.03	3.99	3.84	3.57	3.46
mmol	CH_4	0.16	0.16	0.16	0.15	0.15	0.16	0.16	0.15
	CO_2	0.95	1.13	1.38	1.41	1.59	1.61	1.63	1.61
	C_2H_4	0.05	0.05	0.06	0.05	0.05	0.05	0.04	0.05
	C_2H_6	0.00	0.00	0.00	0.00	0.00	0.00	0.00	0.00
	c atom total	6.25	6.21	6.33	5.64	5.78	5.65	5.40	5.26
% conversion		86.54	84.95	83.65	82.74	84.50	85.78	88.66	88.54
	H_2	27.50	27.25	27.50	25.90	27.36	25.03	23.86	25.04
	CO	77.43	76.43	75.36	75.16	73.09	73.58	72.95	72.87
% selectivity	CH_4	11.64	12.03	12.00	12.09	12.27	12.28	12.62	12.76
	CO_2	5.14	5.01	4.90	4.53	4.95	4.59	4.26	3.88
	C_2H_4	4.08	4.86	5.79	6.23	7.48	7.47	8.07	8.41
	C_2H_6	1.71	1.67	1.96	1.99	2.21	2.09	2.10	2.09

Table B-2 Determination of glycerol conversion and gas product selectivity

Data from the use of catalyst: 10wt%Ni/SiO$_2$, T$_{reaction}$ = 650°C W/G= 6:1 feed flow rate = 0.05 mL/min

Standard gas composition

1%H$_2$ 1%CO 1%CO$_2$ 1%CH$_4$ 1%C$_2$H$_6$ 1%C$_2$H$_4$ Balance in N$_2$

Area	std	2.5	3	3.5	4	4.5	5	5.5	6
H$_2$	94978.15	2518327	2470703	2477801	2458154	2475188	2450547	2499939	2468453
CO	4986.6	118743.8	117419.5	117038.1	114600	114597.3	114616.2	115564.7	114074.8
CH$_4$	19907.8	39870.4	39952	39181.85	41540.9	41462.65	44616.45	49766.4	43614.6
CO$_2$	7588.7	26330.2	24847.9	26011.15	23941.7	23509.8	23663.9	21917.5	20347
C$_2$H$_4$	16703.35	12855	18011.65	21663.45	24647.7	25501.65	28296.8	30436.4	30358.6
C$_2$H$_6$	18458.55	2971.4	2858.05	3492.45	4028.3	3936.7	4351.8	4757	4706.05

	Hour	2.5	3	3.5	4	4.5	5	5.5	6
	H$_2$	9.06	9.38	9.27	9.58	9.73	9.25	9.38	9.47
	CO	8.19	8.55	8.39	8.55	8.68	8.34	8.33	8.42
	CH$_4$	0.69	0.72	0.70	0.77	0.78	0.80	0.89	0.80
mmol	CO$_2$	1.36	1.40	1.41	1.36	1.35	1.31	1.20	1.18
	C$_2$H$_4$	0.53	0.77	0.92	1.08	1.12	1.20	1.28	1.28
	C$_2$H$_6$	0.11	0.11	0.13	0.16	0.16	0.17	0.18	0.18
	c atom total	10.87	11.56	11.56	11.93	12.09	11.82	11.89	11.86
% conversion		57.82	61.52	61.48	63.48	64.34	62.90	63.23	63.08
	H$_2$	36.74	35.91	35.48	35.35	35.53	34.38	34.44	34.99
	CO	75.57	74.02	72.52	71.40	71.37	70.21	69.62	70.68
% selectivity	CH$_4$	6.50	6.56	6.31	6.75	6.73	7.06	7.81	6.97
	CO$_2$	11.98	11.40	11.63	10.85	10.62	10.55	9.68	9.38
	C$_2$H$_4$	4.90	7.01	8.32	9.59	9.91	10.69	11.30	11.37
	C$_2$H$_6$	1.05	1.02	1.22	1.41	1.38	1.48	1.60	1.60

Table B-3 Determination of glycerol conversion and gas product selectivity

Data from the use of catalyst: 10wt%Ni/SiO$_2$, T$_{reaction}$ = 550°C W/G= 6:1 feed flow rate = 0.05 mL/min

Standard gas composition

1%H$_2$ 1%CO 1%CO$_2$ 1%CH$_4$ 1%C$_2$H$_6$ 1%C$_2$H$_4$ Balance in N$_2$

Area	std	2.5	3	3.5	4	4.5	5	5.5	6
H$_2$	93625.3	2454701	2405090	2549470	2427528	2438042	2404285	2372683	2404000
CO	4949	84354.6	80075.5	77401.75	66822.6	64755.6	61990.1	57736.9	57027.8
CH$_4$	19453	10209.2	10169.25	10417.6	9782.4	9762.2	9877.9	9985.8	9417.25
CO$_2$	7761.5	24694.35	29031.45	35377.85	36671.5	40812.15	40840.35	41538.2	41873.05
C$_2$H$_4$	16612.7	1292.6	1418.85	1616.95	1350.45	1264.95	1250.55	1108.55	1281.8
C$_2$H$_6$	18342.1	0	0	0	0	0	0	0	0

Hour		2.5	3	3.5	4	4.5	5	5.5	6
	H$_2$	10.44	10.15	10.09	9.40	10.14	9.42	9.28	9.72
	CO	12.59	12.20	11.85	11.69	11.61	11.86	12.16	12.13
mmol	CH$_4$	1.89	1.92	1.89	1.88	1.95	1.98	2.10	2.12
	CO$_2$	0.84	0.80	0.77	0.70	0.79	0.74	0.71	0.65
	C$_2$H$_4$	0.66	0.78	0.91	0.97	1.19	1.20	1.34	1.40
	C$_2$H$_6$	0.28	0.27	0.31	0.31	0.35	0.34	0.35	0.35
	c atom total	16.27	15.97	15.72	15.55	15.88	16.12	16.66	16.64
% conversion		33.27	33.05	33.70	29.99	30.74	30.04	28.73	28.01
	H$_2$	53.65	53.10	55.57	58.90	58.83	59.82	61.56	62.75
	CO	81.55	78.50	74.76	71.41	68.76	67.70	65.94	65.55
% selectivity	CH$_4$	2.52	2.56	2.57	2.66	2.64	2.74	2.90	2.75
	CO$_2$	15.19	18.10	21.73	25.07	27.79	28.73	30.40	30.80
	C$_2$H$_4$	0.74	0.84	0.94	0.86	0.80	0.82	0.76	0.90
	C$_2$H$_6$	0.00	0.00	0.00	0.00	0.00	0.00	0.00	0.00

Table B-4 Determination of glycerol conversion and gas product selectivity

Data from the use of catalyst: 10wt%Ni/SiO₂, $T_{reaction}$ = 550°C W/G= 6:1 feed flow rate = 0.03 mL/min

Standard gas composition

1%H_2 1%CO 1%CO_2 1%CH_4 1%C_2H_6 1%C_2H_4 Balance in N_2

Area	std	2.5	3	3.5	4	4.5	5	5.5	6
H_2	96249.25	2281397	2191629	2327883	2271885	2308267	2310294	2319159	2282919
CO	5066.35	84109.75	73350.65	75688.6	73791.7	73774.6	71449.65	70115.4	68014.4
CH_4	20026.65	13879.65	12794.85	12741.05	12491.9	12513.2	11083	10684	10371.05
CO_2	7056.2	26863.55	29050.6	30337.7	30683.25	30813.95	32287.45	34254.95	34932.7
C_2H_4	16661.05	1070.3	1141.25	1436.85	1108.7	1330.9	1150.3	1110.15	1113.1
C_2H_6	19149.7	0	0	0	0	0	0	0	0

	Hour	2.5	3	3.5	4	4.5	5	5.5	6
	H_2	6.97	6.90	7.29	7.09	7.29	7.22	7.31	7.32
	CO	4.87	4.40	4.52	4.39	4.43	4.25	4.20	4.14
mmol	CH_4	0.20	0.20	0.20	0.19	0.19	0.17	0.16	0.16
	CO_2	1.12	1.26	1.31	1.32	1.35	1.39	1.48	1.54
	C_2H_4	0.04	0.04	0.06	0.04	0.05	0.04	0.04	0.04
	C_2H_6	0.00	0.00	0.00	0.00	0.00	0.00	0.00	0.00
	c atom total	6.23	5.90	6.08	5.94	6.03	5.85	5.89	5.89
% conversion		55.26	52.32	53.89	52.68	53.45	51.91	52.22	52.19
	H_2	49.10	50.22	51.73	51.39	52.08	52.98	53.20	53.32
	CO	78.09	74.68	74.54	74.03	73.84	72.72	71.37	70.47
% selectivity	CH_4	3.17	3.31	3.16	3.17	3.16	2.88	2.78	2.75
	CO_2	18.21	21.29	21.45	22.12	22.18	23.68	25.13	26.07
	C_2H_4	0.54	0.72	0.85	0.68	0.81	0.73	0.71	0.71
	C_2H_6	0.00	0.00	0.00	0.00	0.00	0.00	0.00	0.00

Table B-5 Determination of glycerol conversion and gas product selectivity

Data from the use of catalyst: 10wt%Ni/SiO$_2$, T$_{reaction}$ = 550°C W/G= 6:1 feed flow rate = 0.01 mL/min

Standard gas composition

1%H$_2$ 1%CO 1%CO$_2$ 1%CH$_4$ 1%C$_2$H$_6$ 1%C$_2$H$_4$ Balance in N$_2$

Area	std	2.5	3	3.5	4	4.5	5	5.5	6
H$_2$	97253.5	1419209	1404493	1466423	1435010	1481266	1464618	1472535	1473529
CO	5000.5	43514.65	43500.85	45852.6	45117.65	46373.95	46013.45	46763	46446.25
CH$_4$	19599.1	12757.95	11656.55	11335.65	11258.25	11426.2	11393.7	11680.6	11769.85
CO$_2$	9862	20217.7	20693.2	21614.85	22240.45	22208.5	23780.35	23330.5	22458.85
C$_2$H$_4$	17048.2	0	0	0	0	0	0	0	0
C$_2$H$_6$	18755.3	0	0	0	0	0	0	0	0

Hour		2.5	3	3.5	4	4.5	5	5.5	6
	H$_2$	3.12	3.11	1.62	3.27	1.64	1.08	1.66	1.65
	CO	1.86	1.87	0.98	2.00	1.00	0.66	1.02	1.01
mmol	CH$_4$	0.14	0.13	0.06	0.13	0.06	0.04	0.07	0.07
	CO$_2$	0.44	0.45	0.24	0.50	0.24	0.17	0.26	0.25
	C$_2$H$_4$	0.00	0.00	0.00	0.00	0.00	0.00	0.00	0.00
	C$_2$H$_6$	0.00	0.00	0.00	0.00	0.00	0.00	0.00	0.00
	c atom total	2.43	2.45	1.28	2.63	1.31	0.88	1.35	1.33
% conversion		64.72	65.11	68.21	70.02	69.54	69.99	71.66	70.65
	H$_2$	54.60	53.99	53.60	53.01	53.48	52.43	52.19	52.93
	CO	76.44	76.55	76.93	76.27	76.77	75.49	76.07	76.62
% selectivity	CH$_4$	5.75	5.26	4.94	4.97	4.96	4.90	4.95	5.07
	CO$_2$	17.81	18.18	18.13	18.76	18.27	19.61	18.98	18.31
	C$_2$H$_4$	0.00	0.00	0.00	0.00	0.00	0.00	0.00	0.00
	C$_2$H$_6$	0.00	0.00	0.00	0.00	0.00	0.00	0.00	0.00

Table B-6 Determination of glycerol conversion and gas product selectivity

Data from the use of catalyst: 10wt%Ni/SiO$_2$, T$_{reaction}$ = 550°C W/G= 3:1 feed flow rate = 0.01 mL/min

Standard gas composition

1%H$_2$ 1%CO 1%CO$_2$ 1%CH$_4$ 1%C$_2$H$_6$ 1%C$_2$H$_4$ Balance in N$_2$

Area	std	2.5	3	3.5	4	4.5	5	5.5	6
H$_2$	99562.6	1712807	1711573	1771811	1626942	1492805	1534748	1409024	1475803
CO	5156.3	85671.1	85372.3	86579.7	76481.5	65904.6	62056.8	53018.9	53055.9
CH$_4$	20745	13222.9	15086.3	15944	14378.5	13730.8	13424.3	11892.7	12607.7
CO$_2$	9488.1	8737.8	11739.1	12307.3	11193.6	11754.8	13106.3	13580.8	16306.7
C$_2$H$_4$	17586.4	0	0	1370	1340.5	1751.6	2137	2157.6	2351.4
C$_2$H$_6$	19109.1	0	0	0	0	0	0	0	0

Hour		2.5	3	3.5	4	4.5	5	5.5	6
	H$_2$	4.28	4.36	4.22	3.91	3.63	1.28	3.58	3.67
	CO	4.14	4.20	3.98	3.55	3.10	1.00	2.60	2.55
	CH$_4$	0.16	0.18	0.18	0.17	0.16	0.05	0.14	0.15
mmol	CO$_2$	0.23	0.31	0.31	0.28	0.30	0.11	0.36	0.43
	C$_2$H$_4$	0.00	0.00	0.04	0.02	0.05	0.01	0.03	0.03
	C$_2$H$_6$	0.00	0.00	0.00	0.00	0.00	0.00	0.00	0.00
	c atom total	4.53	4.69	4.50	4.02	3.61	1.18	3.14	3.16
% conversion		68.79	71.34	68.47	61.08	54.83	53.81	47.67	47.99
	H$_2$	40.57	39.78	40.11	41.73	43.18	46.57	48.87	49.82
	CO	91.43	89.39	88.32	88.39	85.89	84.84	82.86	80.69
% selectivity	CH$_4$	3.51	3.93	4.04	4.13	4.45	4.56	4.62	4.77
	CO$_2$	5.07	6.68	6.82	7.03	8.33	9.74	11.53	13.48
	C$_2$H$_4$	0.00	0.00	0.82	0.45	1.34	0.86	0.99	1.07
	C$_2$H$_6$	0.00	0.00	0.00	0.00	0.00	0.00	0.00	0.00

Table B-7 Determination of glycerol conversion and gas product selectivity

Data from the use of catalyst: 10wt%Ni/SiO$_2$, T$_{reaction}$ = 550°C W/G= 9:1 feed flow rate = 0.01 mL/min

Standard gas composition

1%H$_2$ 1%CO 1%CO$_2$ 1%CH$_4$ 1%C$_2$H$_6$ 1%C$_2$H$_4$ Balance in N$_2$

Area	std	2.5	3	3.5	4	4.5	5	5.5	6
H$_2$	99562.6	1439032	1482590.6	1433252	1447019.6	1388019	1422839	1415758.1	1415209.8
CO	5156.3	39127	39339.8	40949.5	41318.8	40896.1	40527.7	39802.1	39307.1
CH$_4$	20745	6932.5	7556.8	7128.9	6765.9	6645.8	6272.3	5978.9	6113.6
CO$_2$	9488.1	17146.8	15929.3	15741.6	15913.6	15748.4	17141.1	18082.1	19983.1
C$_2$H$_4$	17586.4	0	0	0	0	0	0	0	0
C$_2$H$_6$	19109.1	0	0	0	0	0	0	0	0

	Hour	2.5	3	3.5	4	4.5	5	5.5	6
	H$_2$	3.55	3.73	3.56	3.63	3.49	1.16	3.49	3.45
	CO	1.86	1.91	1.97	2.00	1.99	0.64	1.89	1.85
mmol	CH$_4$	0.08	0.09	0.09	0.08	0.08	0.02	0.07	0.07
	CO$_2$	0.44	0.42	0.41	0.42	0.42	0.15	0.47	0.51
	C$_2$H$_4$	0.00	0.00	0.00	0.00	0.00	0.00	0.00	0.00
	C$_2$H$_6$	0.00	0.00	0.00	0.00	0.00	0.00	0.00	0.00
	c atom total	2.39	2.42	2.46	2.50	2.48	0.81	2.43	2.43
% conversion		90.75	91.96	93.55	94.96	94.32	92.61	92.46	92.45
	H$_2$	63.67	65.98	62.04	62.18	60.28	61.44	61.48	60.77
%	CO	77.99	78.88	79.86	80.00	80.02	78.84	77.87	76.05
selectivity	CH$_4$	3.43	3.77	3.46	3.26	3.23	3.03	2.91	2.94
	CO$_2$	18.57	17.36	16.68	16.74	16.75	18.12	19.22	21.01
	C$_2$H$_4$	0.00	0.00	0.00	0.00	0.00	0.00	0.00	0.00
	C$_2$H$_6$	0.00	0.00	0.00	0.00	0.00	0.00	0.00	0.00

Table B-8 Determination of glycerol conversion and gas product selectivity

Data from the use of catalyst: 5wt%Ni/SiO$_2$, T$_{reaction}$ = 550°C W/G= 9:1 feed flow rate = 0.01 mL/min

Standard gas composition

1%H$_2$ 1%CO 1%CO$_2$ 1%CH$_4$ 1%C$_2$H$_6$ 1%C$_2$H$_4$ Balance in N$_2$

Area	std	2.5	3	3.5	4	4.5	5	5.5	6
H$_2$	91611.8	1250851	1308961	1295329	1242361	1262530	1248802	1225307	1284641
CO	5629.2	44053.2	43768	42086.4	41013.7	39119.1	38609.3	37704.2	40864.2
CH$_4$	21299.9	9202.2	9857.5	9435.9	10040.5	12430.4	10990.1	10364.4	10047.7
CO$_2$	11091.2	11266.9	13720	14178.7	12863.8	16711.7	18594.1	20338.6	21044.2
C$_2$H$_4$	14705.8	0	0	0	0	0	0	0	0
C$_2$H$_6$	19344.5	0	0	0	0	0	0	0	0

Hour		2.5	3	3.5	4	4.5	5	5.5	6
	H$_2$	3.10	3.11	2.98	2.93	2.87	0.95	2.78	2.84
	CO	1.52	1.54	1.62	1.61	1.57	0.52	1.54	1.58
	CH$_4$	0.09	0.09	0.09	0.09	0.10	0.03	0.09	0.09
mmol	CO$_2$	0.16	0.21	0.22	0.20	0.23	0.09	0.28	0.29
	C$_2$H$_4$	0.00	0.00	0.00	0.00	0.00	0.00	0.00	0.00
	C$_2$H$_6$	0.00	0.00	0.00	0.00	0.00	0.00	0.00	0.00
	c atom total	1.77	1.84	1.92	1.90	1.91	0.64	1.92	1.97
% conversion		67.13	70.03	73.03	72.30	72.46	73.28	72.86	74.69
	H$_2$	76.02	72.31	66.51	65.92	64.45	63.61	62.16	61.95
	CO	85.99	83.76	84.14	84.45	82.20	81.38	80.06	80.15
% selectivity	CH$_4$	4.89	4.80	4.58	4.80	5.35	5.06	4.90	4.67
	CO$_2$	9.13	11.45	11.27	10.74	12.45	13.56	15.04	15.18
	C$_2$H$_4$	0.00	0.00	0.00	0.00	0.00	0.00	0.00	0.00
	C$_2$H$_6$	0.00	0.00	0.00	0.00	0.00	0.00	0.00	0.00

Table B-9 Determination of glycerol conversion and gas product selectivity

Data from the use of catalyst: 20wt%Ni/SiO$_2$, T$_{reaction}$ = 550°C W/G= 9:1 feed flow rate = 0.01 mL/min

Standard gas composition

1%H$_2$ 1%CO 1%CO$_2$ 1%CH$_4$ 1%C$_2$H$_6$ 1%C$_2$H$_4$ Balance in N$_2$

Area	std	2.5	3	3.5	4	4.5	5	5.5	6
H$_2$	91611.8	961096	979771.8	1010531.4	1053867.1	1086087.7	1092159.1	1092416.8	1072138
CO	5629.2	23373.1	23130.4	24928.3	26089.1	27324.5	28084.5	29507.3	28975
CH$_4$	21299.9	3883.9	3471.9	3830.9	3813.1	4380.1	3820.2	4448	3833.2
CO$_2$	11091.2	15777.2	14606.8	13388.6	13581.8	12523.1	12309.7	12124.1	12054.4
C$_2$H$_4$	14705.8	0	0	0	0	0	0	0	0
C$_2$H$_6$	19344.5	0	0	0	0	0	0	0	0

Hour		2.5	3	3.5	4	4.5	5	5.5	6
	H$_2$	2.69	2.71	2.85	2.97	3.05	1.00	2.99	2.94
	CO	1.07	1.04	1.14	1.20	1.25	0.42	1.31	1.29
	CH$_4$	0.05	0.04	0.05	0.05	0.05	0.02	0.05	0.05
mmol	CO$_2$	0.36	0.33	0.31	0.32	0.29	0.09	0.27	0.27
	C$_2$H$_4$	0.00	0.00	0.00	0.00	0.00	0.00	0.00	0.00
	C$_2$H$_6$	0.00	0.00	0.00	0.00	0.00	0.00	0.00	0.00
	c atom total	1.48	1.42	1.50	1.56	1.59	0.53	1.64	1.61
% conversion		32.06	40.03	56.77	57.96	56.77	56.68	59.32	60.72
	H$_2$	98.80	90.65	80.77	79.17	79.34	79.42	77.89	77.82
	CO	70.49	73.47	72.55	72.51	70.76	69.70	70.57	69.26
% selectivity	CH$_4$	3.78	3.25	3.54	3.36	3.61	3.10	2.99	2.78
	CO$_2$	25.73	23.27	23.91	24.13	25.63	27.20	26.44	27.96
	C$_2$H$_4$	0.00	0.00	0.00	0.00	0.00	0.00	0.00	0.00
	C$_2$H$_6$	0.00	0.00	0.00	0.00	0.00	0.00	0.00	0.00

Table B-10 Determination of glycerol conversion and gas product selectivity

Data from the use of catalyst: 1wt%Ce-10wt%Ni/SiO$_2$, T$_{reaction}$ = 550°C W/G= 9:1 feed flow rate = 0.01 mL/min

Standard gas composition

1%H$_2$ 1%CO 1%CO$_2$ 1%CH$_4$ 1%C$_2$H$_6$ 1%C$_2$H$_4$ Balance in N$_2$

Area	std	2.5	3	3.5	4	4.5	5	5.5	6
H$_2$	99562.6	1475956	1395252	1481125	1395362	1352624	1313358	1257675	1244790
CO	5156.3	28626.6	29654.5	30852.4	31312.6	31133.7	30331	30939.7	30746.3
CH$_4$	20745	6259.4	6127.6	6155.5	6693.2	6600.9	6922.4	6698	6888.6
CO$_2$	9488.1	10875.4	12482.3	17852.9	18938.9	18771.3	21740.4	22054.6	22628.6
C$_2$H$_4$	17586.4	0	0	0	0	0	0	0	0
C$_2$H$_6$	19109.1	0	0	0	0	0	0	0	0

Hour		2.5	3	3.5	4	4.5	5	5.5	6
	H$_2$	3.39	3.17	3.28	3.20	3.06	0.99	2.81	2.79
	CO	1.27	1.30	1.32	1.39	1.36	0.44	1.34	1.33
mmol	CH$_4$	0.07	0.07	0.07	0.07	0.07	0.03	0.07	0.07
	CO$_2$	0.26	0.30	0.41	0.46	0.44	0.17	0.52	0.53
	C$_2$H$_4$	0.00	0.00	0.00	0.00	0.00	0.00	0.00	0.00
	C$_2$H$_6$	0.00	0.00	0.00	0.00	0.00	0.00	0.00	0.00
	c atom total	1.60	1.67	1.80	1.92	1.87	0.64	1.92	1.94
% conversion		60.83	63.31	68.40	72.86	71.23	72.91	73.13	73.61
	H$_2$	90.77	81.58	78.11	71.58	69.86	66.45	62.60	61.73
	CO	79.31	78.12	73.31	72.37	72.44	69.14	69.39	68.70
% selectivity	CH$_4$	4.31	4.01	3.64	3.84	3.82	3.92	3.73	3.83
	CO$_2$	16.38	17.87	23.05	23.79	23.74	26.93	26.88	27.48
	C$_2$H$_4$	0.00	0.00	0.00	0.00	0.00	0.00	0.00	0.00
	C$_2$H$_6$	0.00	0.00	0.00	0.00	0.00	0.00	0.00	0.00

Table B-11 Determination of glycerol conversion and gas product selectivity

Data from the use of catalyst: 2wt%wt-10wt%Ni/SiO$_2$, T$_{reaction}$ = 550°C W/G= 6:1 feed flow rate = 0.01 mL/min

Standard gas composition

1%H$_2$ 1%CO 1%CO$_2$ 1%CH$_4$ 1%C$_2$H$_6$ 1%C$_2$H$_4$ Balance in N$_2$

Area	std	2.5	3	3.5	4	4.5	5	5.5	6
H$_2$	99562.6	1392108	1371541	1350422	1359832	1396118	1403918	1266529	1197383
CO	5156.3	28988.3	27795.1	28520.8	27360.2	27159	27830.3	25181.3	25246.6
CH$_4$	20745	10769.5	10503.9	10462.5	10686.9	9792.9	9332.5	7873.5	7259.2
CO$_2$	9488.1	13361.3	16889.5	20110.3	24041.8	26971.4	28868.6	31295.3	30858
C$_2$H$_4$	17586.4	0	0	0	0	0	0	0	0
C$_2$H$_6$	19109.1	0	0	0	0	0	0	0	0

	Hour	2.5	3	3.5	4	4.5	5	5.5	6
	H$_2$	2.94	2.84	2.83	2.88	2.97	0.98	2.68	2.56
	CO	1.18	1.11	1.15	1.12	1.11	0.38	1.03	1.04
mmol	CH$_4$	0.11	0.10	0.11	0.11	0.10	0.03	0.08	0.07
	CO$_2$	0.30	0.37	0.44	0.53	0.60	0.21	0.70	0.69
	C$_2$H$_4$	0.00	0.00	0.00	0.00	0.00	0.00	0.00	0.00
	C$_2$H$_6$	0.00	0.00	0.00	0.00	0.00	0.00	0.00	0.00
	c atom total	1.59	1.58	1.70	1.76	1.82	0.62	1.81	1.81
% conversion		60.38	60.09	64.63	66.93	69.02	70.77	68.64	68.87
	H$_2$	79.38	76.90	71.28	70.06	70.03	67.98	63.68	60.65
	CO	74.47	70.22	67.83	63.51	61.38	60.71	57.04	57.61
% selectivity	CH$_4$	6.88	6.60	6.18	6.17	5.50	5.06	4.43	4.12
	CO$_2$	18.65	23.19	25.99	30.33	33.12	34.23	38.53	38.27
	C$_2$H$_4$	0.00	0.00	0.00	0.00	0.00	0.00	0.00	0.00
	C$_2$H$_6$	0.00	0.00	0.00	0.00	0.00	0.00	0.00	0.00

Table B-12 Determination of glycerol conversion and selectivity Reaction Product

Data from the use of catalyst: 10wt%Ni/SiO$_2$ porous catalyst, T$_{reaction}$ = 550°C W/G= 6:1 feed flow rate = 0.01 mL/min

Standard gas composition

1%H$_2$ 1%CO 1%CO$_2$ 1%CH$_4$ 1%C$_2$H$_6$ 1%C$_2$H$_4$ Balance in N$_2$

Area	std	2.5	3	3.5	4	4.5	5	5.5	6
H$_2$	95844.6	1758931	1728546	1769984	1788997	1757544	1754975	1737200	1749463
CO	4791	15495.8	10851.1	12734.3	12680.7	12137.1	12703.6	12339.5	11216.8
CH$_4$	20080.9	23920.9	17297.5	13042.7	15796.6	15952.4	15775.6	14374.7	14343.2
CO$_2$	9030	39860.3	47816.3	48262.9	50604.5	49390.1	50186.5	50003.3	50846.3
C$_2$H$_4$	16560.4								
C$_2$H$_6$	19339.2								

	Hour	2.5	3	3.5	4	4.5	5	5.5	6
	H$_2$	4.12	4.03	4.16	4.20	4.18	4.14	4.12	4.18
	CO	0.73	0.51	0.60	0.60	0.58	0.60	0.59	0.54
	CH$_4$	0.27	0.19	0.15	0.18	0.18	0.18	0.16	0.16
mmol	CO$_2$	0.99	1.18	1.21	1.26	1.25	1.26	1.26	1.29
	C$_2$H$_4$	0.00	0.00	0.00	0.00	0.00	0.00	0.00	0.00
	C$_2$H$_6$	0.00	0.00	0.00	0.00	0.00	0.00	0.00	0.00
	c atom total	1.99	1.88	1.95	2.03	2.00	0.68	2.01	1.99
% conversion		75.44	71.46	74.15	77.28	76.12	77.26	76.22	75.66
	H$_2$	88.97	91.78	91.47	88.52	89.33	87.24	87.98	90.06
	CO	36.59	26.89	30.72	29.29	28.80	29.48	29.17	26.95
%	CH$_4$	13.48	10.23	7.51	8.70	9.03	8.73	8.11	8.22
selectivity	CO$_2$	49.94	62.88	61.77	62.01	62.17	61.79	62.72	64.82
	C$_2$H$_4$	0.00	0.00	0.00	0.00	0.00	0.00	0.00	0.00
	C$_2$H$_6$	0.00	0.00	0.00	0.00	0.00	0.00	0.00	0.00

VITA

Miss Nattida Tangkanaporn was born on January 22, 1985 in Chonburi, Thailand. She graduated with Bachelor's degree of Science, majoring in Biochemistry, Faculty of Science, Chulalongkorn University in 2007. She has continued her study in Master's degree, majoring in Petrochemistry and Polymer Science, Faculty of Science, Chulalongkorn University, Bangkok, Thailand since 2007 and finished her study in 2009.

Presentation Experience

Oral presentation from The Pure and Applied Chemistry Conference (PACCON2009) which organized by Naresoun University in the topic of "Glycerol steam reforming over Ni/SiO_2 fiber catalysts prepared by electrospinning technique".